NAVAL POSTGRADUATE SCHOOL

MONTEREY, CALIFORNIA

THESIS

PREDICTING WAVE-INDUCED LOADS IN COMPLEX SEAWAYS ON SHALLOWLY SUBMERGED VESSELS

by

Andrew R. Whitmer

June 2018

Thesis Advisor: Joseph Klamo
Second Reader: Fotis A. Papoulias

Approved for public release. Distribution is unlimited.

THIS PAGE INTENTIONALLY LEFT BLANK

REPORT DOCUMENTATION PAGE	*Form Approved OMB No. 0704-0188*

1. AGENCY USE ONLY *(Leave blank)*	**2. REPORT DATE** June 2018	**3. REPORT TYPE AND DATES COVERED** Master's thesis

4. TITLE AND SUBTITLE PREDICTING WAVE-INDUCED LOADS IN COMPLEX SEAWAYS ON SHALLOWLY SUBMERGED VESSELS	**5. FUNDING NUMBERS**
6. AUTHOR(S) Andrew R. Whitmer	
7. PERFORMING ORGANIZATION NAME(S) AND ADDRESS(ES) Naval Postgraduate School Monterey, CA 93943-5000	**8. PERFORMING ORGANIZATION REPORT NUMBER**
9. SPONSORING / MONITORING AGENCY NAME(S) AND ADDRESS(ES) N/A	**10. SPONSORING / MONITORING AGENCY REPORT NUMBER**

11. SUPPLEMENTARY NOTES The views expressed in this thesis are those of the author and do not reflect the official policy or position of the Department of Defense or the U.S. Government.

12a. DISTRIBUTION / AVAILABILITY STATEMENT Approved for public release. Distribution is unlimited.	**12b. DISTRIBUTION CODE** A

13. ABSTRACT (maximum 200 words)

This thesis analyzes the validity of using linear superposition to accurately predict the forces and moments on a shallowly submerged vessel in a complex seaway. Linear superposition implies that the forces and moments due to the complex seaway are simply the summation of the forces and moments of the single regular waves that combine to create the complex seaway. The forces and moments are measured on a UUV-shaped model in the tow tank with wave making capability at the Naval Postgraduate School with the aid of various data collection processes. First, the forces and moments due to single regular waves are studied. Single regular wave results are then combined to predict what complex waveform loads would be and the accuracy is assessed. The results show that linear superposition is a valid assumption over the wave heights and frequencies tested, especially for wavelengths greater than the length of the submerged body when the submerged depth is twice the diameter of the body.

14. SUBJECT TERMS wave-induced loads, near surface operation, shallowly submerged vehicle, multi-component seaway, linear superposition, load predictions	**15. NUMBER OF PAGES** 71
	16. PRICE CODE

17. SECURITY CLASSIFICATION OF REPORT	**18. SECURITY CLASSIFICATION OF THIS PAGE**	**19. SECURITY CLASSIFICATION OF ABSTRACT**	**20. LIMITATION OF ABSTRACT**
Unclassified	Unclassified	Unclassified	UU

NSN 7540-01-280-5500 Standard Form 298 (Rev. 2-89) Prescribed by ANSI Std. 239-18

THIS PAGE INTENTIONALLY LEFT BLANK

Approved for public release. Distribution is unlimited.

PREDICTING WAVE-INDUCED LOADS IN COMPLEX SEAWAYS ON SHALLOWLY SUBMERGED VESSELS

Andrew R. Whitmer
Lieutenant, United States Navy
BS, University of Tennessee, 2009

Submitted in partial fulfillment of the
requirements for the degree of

MASTER OF SCIENCE IN SYSTEMS ENGINEERING

from the

NAVAL POSTGRADUATE SCHOOL
June 2018

Approved by: Joseph Klamo
Advisor

Fotis A. Papoulias
Second Reader

Ronald E. Giachetti
Chair, Department of Systems Engineering

THIS PAGE INTENTIONALLY LEFT BLANK

ABSTRACT

This thesis analyzes the validity of using linear superposition to accurately predict the forces and moments on a shallowly submerged vessel in a complex seaway. Linear superposition implies that the forces and moments due to the complex seaway are simply the summation of the forces and moments of the single regular waves that combine to create the complex seaway. The forces and moments are measured on a UUV-shaped model in the tow tank with wave making capability at the Naval Postgraduate School with the aid of various data collection processes. First, the forces and moments due to single regular waves are studied. Single regular wave results are then combined to predict what complex waveform loads would be and the accuracy is assessed. The results show that linear superposition is a valid assumption over the wave heights and frequencies tested, especially for wavelengths greater than the length of the submerged body when the submerged depth is twice the diameter of the body.

THIS PAGE INTENTIONALLY LEFT BLANK

Table of Contents

List of Figures

List of Tables

THIS PAGE INTENTIONALLY LEFT BLANK

List of Acronyms and Abbreviations

NPS	Naval Postgraduate School
USN	U.S. Navy
USB	Universal Serial Bus
UUVs	unmanned underwater vehicles
Hz	Hertz
GUI	graphical user interface
RAO	response amplitude operator

THIS PAGE INTENTIONALLY LEFT BLANK

Executive Summary

The goal of this thesis is to better predict the wave-induced loads on a shallowly submerged vessel in a realistic complex seaway. Because we cannot simulate every complex wave environment that operational unmanned underwater vehicles (UUVs) could possibly encounter, it is necessary to use the more basic information from single waves to predict the loads on the vessel. To answer this question the tow tank with wave making capabilities at the Naval Postgraduate School (NPS) is utilized. The general experimental approach is to measure the forces and moments exerted on a shallowly submerged vessel due to single regular waves passing over it. Multiple combinations of these single regular waves are then produced to make more complex wave environments. Assuming linear superposition is valid, the forces and moments on the shallowly submerged vessel due to the complex wave environment are simply a sum of the forces and moments due to the single regular waves contained within the complex wave environment. This thesis attempts to analyze the validity of using linear superposition in such a manner. Our approach is analogous to linear seakeeping theory where the motion responses of a vessel in a complex seaway is predicted by summing the known motion response of the vessel in the individual regular waves that make up the seaway. In our case, however, we are concerned with the loads instead of motion responses. Experimental results are then taken and compared to the predictions for assessing the validity of linear superposition.

This thesis demonstrates that it is valid to use linear superposition to predict the forces and moments on shallowly submerged vessels under a variety of specific conditions. First, all experiments are conducted using a stationary vessel with no forward speed at a submerged center-line depth of twice the diameter of the body. The body used was a 4.5-inch diameter and 45-inch long aluminum cylinder with polycarbonate 3-D printed semi-hemispheric end caps. Wavelengths of 22.5 to 90 inches are analyzed with wave amplitudes of 0.25, 0.50, 0.75, and 1.0 inches. Lastly, combinations of two and three underlying regular waves are studied. Under these conditions, it is possible to predict the forces and moments on shallowly submerged vessels by using knowledge of the loads that result from the underlying individual wave components.

The first phase of the study is to measure the drag force, vertical force, and pitching moment

on a shallowly submerged vessel due to single regular waves. This is done for each of the four wave amplitudes while varying the wavelength incrementally from 22.5 to 90 inches. With this data, load versus non-dimensional wavelength (λ/L) curves are created for each amplitude and load parameter. The multi-wave study begins by combining two of the single regular waves of differing frequency previously studied in order to produce a more complex wave environment. The same parameters of drag force, vertical force, and pitching moment are captured. The loads that result from the complex wave environment are then decomposed to determine the amplitude contribution at the frequencies of the underlying regular waves. Similar force versus non-dimensional wavelength curves are created as to those in the single regular wave study. The plots between the single regular wave and multi-component wave experiments are analyzed to determine the efficacy of using linear superposition for forces and moments. This process is then repeated by combining three of the single regular waves and analyzing as before.

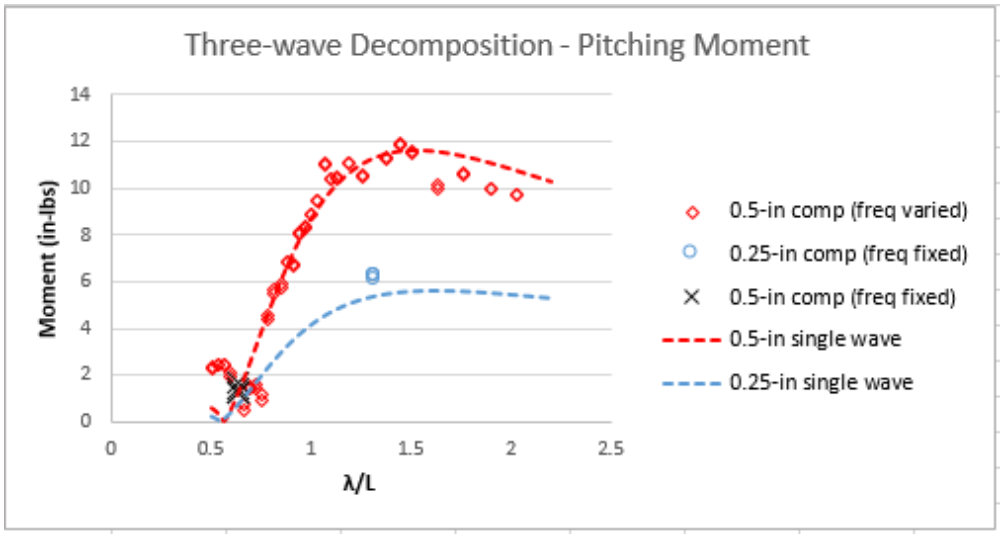

Figure 1. Experimental Irregular Three-wave Pitching Moment

An example of results is shown in Figure 1. In order to create these results, three single regular waves of different frequencies are combined to create a complex wave environment in the tow tank. The load on the body due to the complex wave environment is then measured via a load cell. The load can be decomposed into the contributions associated with each of the frequencies of interest. Figure 1 shows a red dashed line representing the experimental pitching moment versus λ/L curve determined using only 0.5-inch single regular waves and a blue dashed line to represent 0.25-inch single waves. The data markers capture

the results from the complex wave environment containing all three wave components. The red diamond markers show the contribution of the first 0.5-inch wave, which had its wavelength varied, to the pitching moment, and the blue circles represent the contribution of a 0.25-inch wave to the pitching moment. The black cross-hair style markers represent the pitching moment due to the second 0.5-inch wave which is held at constant frequency. If linear superposition is potentially a valid theory, one would expect the red, blue, and black markers to closely align with the results from single regular wave tests. That appears to be the case in this instance.

These results have a variety of applications across many domains. The most direct contribution is to UUV control systems. By better understanding the loads exerted on a shallowly submerged vessel due to realistic complex seaways, it is easier to define design requirements based on the projected operating environment. Overall, it could allow UUVs to conduct sustained near-surface operations, greatly increasing littoral mission sets, the ability to communicate with outside entities, and overall operational efficiency.

THIS PAGE INTENTIONALLY LEFT BLANK

Acknowledgments

I would like to acknowledge Professor Klamo, who guided me along the way as my thesis advisor. Professor Papoulias also reviewed the thesis and provided valuable input. Lieutenant Travis Turner was also incredibly helpful in getting me up to speed on the operation of the tow tank and associated equipment. Without these three, a quality thesis would have been much more difficult to produce.

THIS PAGE INTENTIONALLY LEFT BLANK

CHAPTER 1:
Introduction

The goal of this thesis is to assess the validity of predicting the wave-induced loads in a complex seaway by superimposing the load results from individual regular waves. Since an infinite number of complex seaways exist, it is impossible to directly study each one numerically or experimentally. Thus, it is necessary to use the basic information from single waves to predict the loads on the vessel in a complex seaway. To assess the validity of predicting complex seaways loads using superposition, the tow tank at the Naval Postgraduate School (NPS) is utilized. The general approach is to measure the forces and moments exerted on a shallowly submerged vessel due to single regular waves passing over. Multiple forms of these single regular waves will then be combined to make more complex wave environments. Assuming linear superposition is valid, the forces and moments on the shallowly submerged vessel due to the complex wave environment will simply be a sum of the forces and moments due to the underlying single regular waves.

The term shallowly submerged is used frequently throughout this thesis. The author uses this term to define the situation where the submerged body is close enough to the surface to feel the effects of waves. Historically, this has meant operating at a centerline submerged depth of no more than four or five times the diameter of the body. In this context, this research falls within this range since we tested at a centerline depth of two diameters. This historical rule-of-thumb, however, is lacking since the influence depth of waves actually depends on the wavelength, and this is not captured in the rule-of-thumb. Since this thesis is not interested in determining where the influence becomes negligible, we are not concerned with what is the most appropriate way to characterize depth. Rather, regarding this matter, we are only concerned that we are within the region of wave effects.

If it is possible to predict the loads exerted on a shallowly submerged vessel in a complex seaway accurately, operational limits such as minimum operating depth for unmanned underwater vehicles (UUVs) can be better understood and predicted based on the projected operational environment. This is important because it could help drive design requirements for future UUVs based on the projected operating environment. Furthermore, it could help to provide operational guidance regarding if an existing UUV will be able to perform a

certain mission given its performance capabilities and the current wave environment.

1.1 Research Question

This work will attempt to determine the accuracy of superimposing the load results from single regular wave tests to predict the forces and moments exerted on a shallowly submerged vessel in a realistic complex seaway containing a combination of multiple regular waveforms.

1.2 Motivation

With the increase in littoral operations in both military and civilian applications, submerged bodies are increasingly being required to operate near the surface. Realistic ocean environments, in the littorals and open ocean, are complex and contain many underlying components. Moreover, different locations have vastly different seaways which are constantly changing. Because of this it is necessary to explore the possibility of predicting complex wave-induced loads from a bounded set of regular waves.

Various research efforts have investigated the effects of single regular waves on vessels. These studies have been quite broad and encompassed submerged, partially submerged, and surfaced vessels. They have also covered a variety of depths of submergence on bodies of different cross-sectional area, geometry, and orientation. This study intends to build on previous work by Cummins and others to test the superposition theory. This study is also motivated by linear seakeeping theory and uses the same principles to predict force and moment time histories due to complex seaways. Notably, the concept of the response amplitude operator (RAO) used in linear seakeeping theory will be applied to forces and moments on submerged bodies and tested against experimental results.

1.3 Applications to Systems Engineering

This research has a variety of applications to systems engineering. The most obvious direct effect is on the control systems for UUVs. A generic high-level physical architecture is shown in Figure 1.1.

A general UUV consists of a variety of sub-systems to form the complete system. An example of these sub-systems could be the navigation system, sensors, communication

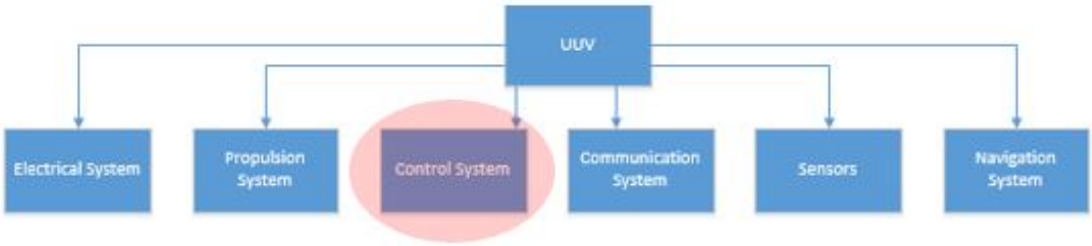

Figure 1.1. Example High-Level UUV Physical Architecture

system, control system, propulsion system, and electrical system. Early on in the preliminary design phase, certain parameters will be allocated to each sub-system. If linear superposition is a valid theory for the forces and moments of shallowly submerged vessels, the control authority requirements can be readily defined based on the projected operating environment since no experiments or simulation would be necessary. As such, the sub-system allocation could be altered based on the control system requirements. This research could ideally lead to the design of more efficient control systems from which all other systems onboard would benefit.

In their current employment, UUVs typically operate deeply submerged during their mission and only operate near the surface during launch and recovery. By better understanding the loads on vessels operating near the surface, it is possible that new mission sets could be defined. For example, this could lead to better defining minimum operating depths based on current sea states or an increase in the ability of the UUVs to communicate with outside entities. It could drive the design of control surfaces to ensure they have the proper control authority to maintain a desired depth. Another possible benefit is the design of model-predictive control algorithms that are able to predict the upcoming wave-induced loads the vehicle will experience to adjust the control surfaces to better compensate for them. Efficiency during energy generation and harvesting operations could also be greatly improved as those craft generally operate near the surface for maximum energy.

Overall, the application to systems engineering is that of a classical trade off analysis. UUVs are generally inherently limited in their size due to launch and recovery requirements and current battery capabilities are insufficient to support long-term sustained operations at sea. By improving the control systems, it is possible that operational durations could be extended, littoral operations could be greatly improved, and requirements could be better

understood early in the design process.

1.4 Methodology

The research question will be answered by conducting a two-phase experimental study utilizing the NPS tow tank. The first phase of the experiment will be to measure the drag force, vertical force, and pitching moment on a submerged body as a result of single regular waves. For each different regular wave amplitude tested, three load versus non-dimensional wavelength (λ/L) curves will be fit for use during the complex wave study.

The multi-wave study will begin by combining two of the single regular waves previously studied in order to produce a more complex wave environment. Drag force, vertical force, and pitching moment will again be measured. The complex load time histories will then be decomposed into the underlying amplitudes at each of the single regular wave frequencies and similar force versus non-dimensional wavelength curves will be created. The plots between the single regular wave and multi-component wave experiments will be analyzed to determine the validity of using linear superposition for predicting the complex forces and moments. This process will then be repeated by combining three of the single regular waves and analyzing as before. Lastly, based on the concept of the RAO used in linear seakeeping theory, this thesis will demonstrate how a complex force time history can be predicted. It involves the use of the RAO to predict the force and moment time histories by knowing the wave amplitude and frequency of the component waves that make up the complex seaway.

1.5 Thesis Organization

This thesis is organized as follows. Chapter II introduces research on single regular waves as well as previous and ongoing research at NPS. Chapter III describes the experimental setup, data collection, and calibration processes. Chapter IV contains the data collection and reduction. Chapter V contains the results and analysis. Chapter VI contains the conclusions, future work, and recommendations.

CHAPTER 2:
Literature Review, Theory, and NPS Research

A number of previous research efforts investigated the loads experienced by bodies in seaways under the influence of surface waves. Before undergoing a study into multiple wave linear superposition, it is important to understand the underlying single wave theory. The goal of this chapter is to introduce some of the research, both analytical and experimental, that can aid in our understanding of single regular waves. It will also highlight some of the previous and concurrent research that the Naval Hydrodynamics Laboratory at NPS has overseen and discusses previous methods for analyzing complex seaways.

2.1 Cummins Research on Single Regular Wave Forces and Moments

The forces and moments on a shallowly submerged vessel due to single regular waves can be predicted according to work put forth by Cummins. The work by Cummins was conducted at the Naval Surface Warfare Center–Carderock Division in the early 1950s. The equations put forth by Cummins apply to a slender body of revolution which is moving at a constant velocity subjected to the effects of sinusoidal waves oblique to the body [1]. For the purposes of this experiment, the relevant equations that are used relate to the drag force, vertical force, and pitching moment. They are presented as Equations 37, 39, and 57, respectively, in the Cummins technical report [1]. Because this experiment is only concerned with a submerged body which has zero forward speed, is oriented head on into the incoming waves, and is symmetric fore and aft, the equations can be reduced from the general form into a more specific form.

The drag force, F_x, can be simplified to

$$F_x = \frac{-\pi}{2}\rho g A_o h(1/\lambda^*)\exp^{-2\pi H'} b_o \cos(\omega_e t), \tag{2.1}$$

where ρ is the fluid density, g is gravitational acceleration, A_o is the cross sectional area at the body midpoint, λ^* is the non-dimensional wavelength, λ/L , H' is the non-dimensional centerline depth of body, H/λ, b_o is an integral expression, and ω_e is the encounter

frequency. This equation tells us that the drag force experienced by the submerged body is directly proportional to fluid density, gravity, cross-sectional area of the body, wave height, and an integral expression that depends on the longitudinal profile curve of the hull geometry. Furthermore, it is dependent on non-dimensional wavelength and depth of the body.

The vertical force equation can be simplified to

$$F_z = -\pi \rho g A_o h (1/\lambda^*) \exp^{-2\pi H'} b_o \sin(\omega_e t). \tag{2.2}$$

This looks quite similar to the simplified drag force equation seen above. The major differences are that the vertical force is greater in magnitude by a factor of two as well as the difference in the sin and cos terms. Simply stated, according to the equations put forth by Cummins, we should expect to see that the vertical force is larger than the drag force. Also, when looking at the time histories of each, the forces should be 90 degrees out of phase with one another.

Lastly, the pitching moment equation can be simplified to

$$M_y = \frac{-\pi}{2} \rho g A_o L h (1/\lambda^*) \exp^{-2\pi H'} a_1 \cos(\omega_e t). \tag{2.3}$$

The pitching moment equation is a bit more complicated than Equations 2.1 and 2.2 due to the functional form of a_1. The two differences are the inclusion of a term for the length of the body, L, and the use of the a_1 vice b_0 integral expression.

These are exact analytic solutions from the idealized mathematical representation of the problem. One example of the mathematical simplification is the assumption of an inviscid fluid. In the actual experiment, we expect our forces and moments to differ somewhat from these expressions. In order to capture these actual loads more accurately, we maintain the functional form of the idealized solutions but allow the prescribed constant terms to be unknown constants that we will solve for. This will be useful later when attempting to calculate curve fit functions based on the general form of the equations. The form of these new equations is as follows.

$$F_x = A \sin\left(\frac{B}{\lambda/L}\right) e^{\frac{C}{\lambda/L}} \tag{2.4}$$

$$F_z = A \sin\left(\frac{B}{\lambda/L}\right) e^{\frac{C}{\lambda/L}} \tag{2.5}$$

$$M_y = A\left(\frac{\lambda}{L}\right)\left(\sin\left(\frac{B}{\lambda/L}\right) + \frac{C}{\lambda/L}\cos\left(\frac{D}{\lambda/L}\right)\right) e^{\frac{C}{\lambda/L}} \tag{2.6}$$

2.2 Other Research on Single Regular Wave Forces and Moments

Khalil [2] conducted research using the tow tank at the University of Tokyo. The focus of his research centered on shallowly submerging cylindrical and rectangular hull forms and varying their depth. The non-dimensional depth of the bodies was varied from 1 to 2.25 and the drag and vertical forces was measured. Notably, Khalil placed the bodies parallel to the incoming waves. Again, for the purposes of this experiment we are only examining cases with head-on waves.

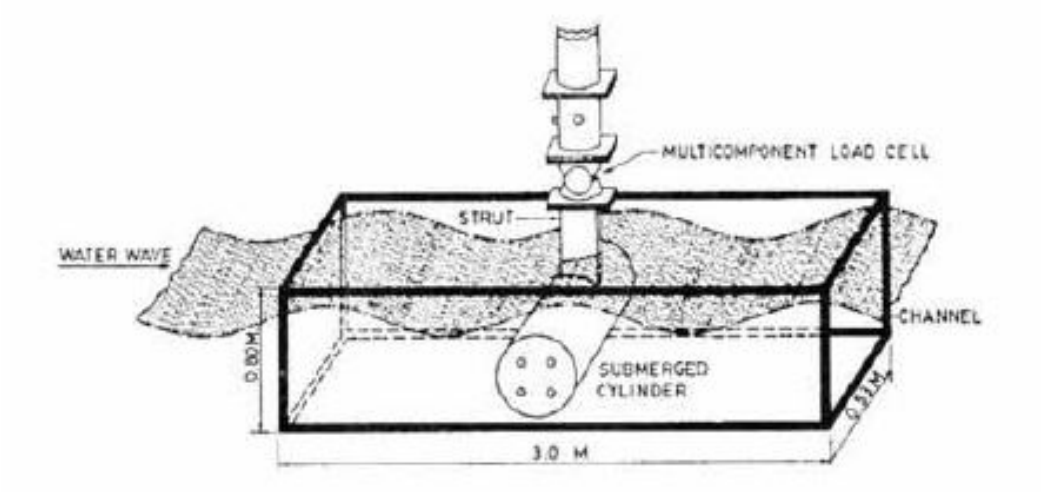

Figure 2.1. Experimental Setup Used by Khalil. Source: [2].

Khalil used this geometry because he was concerned with the effects of waves on off-shore structures. The results of this experiment showed that at shallow enough depths, non-linear effects were observed. This non-linearity is attributed to the breaking waves as

they pass over very shallowly submerged vessels. As Khalil states, "When a wave passes over a shallowly submerged cylinder and breaks behind it, the water particles in that region are naturally decelerated. These decelerated fluid particles exert a high static pressure on the rear side of the cylinder, and as a consequence, it experiences a negative drifting force" [2]. Lastly, Khalil noted that these non-linear wave forces tend to become negligible for non-dimensional depths greater than two.

Ananthakrishnan and Zhang [3] created a nonlinear hydrodynamics model to study the effects of forces when a submerged body is traveling near either the sea floor or the surface of the water. Their results showed an increase in forces when the body is traveling near either boundary [3]. A time history of their results for surface operations is shown in Figure 2.2. Of note, Ananthakrishnan and Zhang used the term heave force to refer to force in the

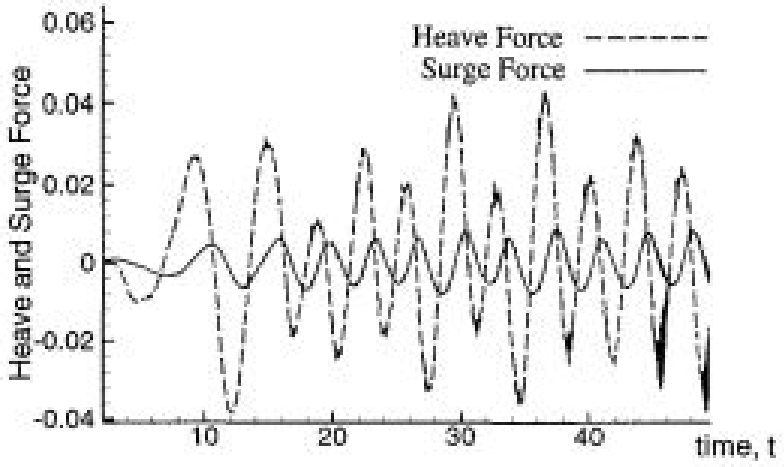

Figure 2.2. Time history of vertical and horizontal wave force components on shallowly submerged UUV. Source: [2].

vertical direction and surge force to refer to the drag force. Ananthakrishnan and Zhang showed through their simulations that slightly submerged bodies should experience large vertical forces when operating near the surface.

Lee and Newman [4] derived equations for the forces and moments on neutrally buoyant submerged bodies under single regular waves. Lee and Newman utilized Kochin functions as opposed to Lagally's theorem which was invoked by Cummins. It appears that the approximations put forth by Lee and Newman only hold for deeply submerged bodies in

infinitely deep water. However, it is postulated in the paper that changes to the geometry of the submerged body will have greater effects on wave-induced loads near the surface [4] .

Pinkster [5] conducted research on the second order forces due to waves acting upon semi-submersible vessels. He derived theoretical expressions for the magnitude of the second order forces and conducted limited experiments to test the theory. Pinkster noted in the study that non-linearity was observed when analyzing waves in the presence of current. These interaction effects were not fully understood and only observed experimentally [5]. The study of only semi-submersibles makes Pinkster's non-linearity observations interesting, but not all that useful in the context of this thesis.

2.3 Traditional Methods for Analyzing Complex Seaways

Traditionally, surface waves in the open ocean are considered to be created as a result of interactions between wind and the water's surface. The wind blowing over the top of the water causes friction between the air and water and produces pressure differences in the air [6]. These two phenomena create local disturbances in the water which then propagate outwards. When propagating, the disturbances interact with others and create a complex wave environment. The traditional way of analyzing the complex wave environment uses linear superposition. That is to say that the amplitude of the complex wave environment at any given time is simply equal to the sum of the amplitudes of the individual component waves. Thus Lewis [6] postulates that the complex wave environment would have the form of the following equation.

$$\xi(x, y, t) = \sum_i \xi_i(x, y, t) \tag{2.7}$$

The principle of linear superposition generally holds, but there are some known limitations. For example, very large steep waves exhibit non-linearity. Another known limitation is that energy tends to appear at the sums and differences of differing frequencies in complex seaways.

Knowing this information, a mathematical model can be created to describe a typical complex seaway shown in Figure 2.3.

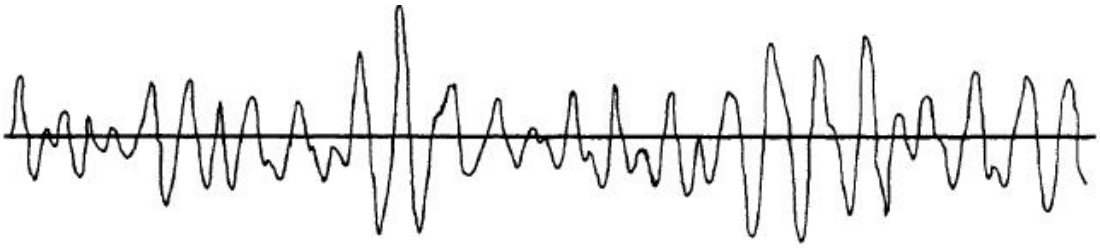

Figure 2.3. Typical Wave Time History of a Complex Seaway. Source: [6].

Lewis [6] derives the following equation to describe such a system.

$$E = \int_0^\infty S(\omega) d\omega \tag{2.8}$$

In Equation 2.8, E is the total variance of the complex wave, $S(\omega)$ is the variance spectrum, and $d\omega$ is the width of each spectrum. The variance spectrum represents the total variance for each particular frequency band. The width of each spectrum determines the accuracy of the calculation. A graphical representation of the integral is shown in the top half of Figure 2.4. The frequency spectrum shown here can be adequately represented using 15 to 20 component waves shown in the bottom half of Figure 2.4 [6].

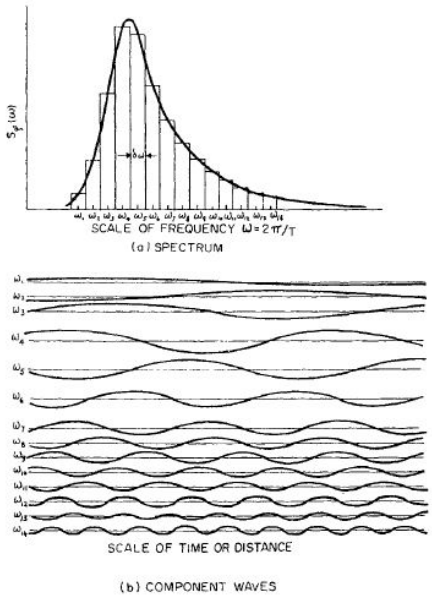

Figure 2.4. Variance Spectrum of Waves. Source: [6].

2.4 Linear Seakeeping Theory

Linear seakeeping theory is used to predict the motion response of a surface vessel while in the presence of a complex seaway. In order to define the predicted response of a ship in a seaway, the so called RAO is used. The RAO is essentially a transfer function that relates a certain response of interest, such as roll, to a certain wave frequency, with unit amplitude [6]. A use case summary of an RAO transfer function is provided in Figure 2.5.

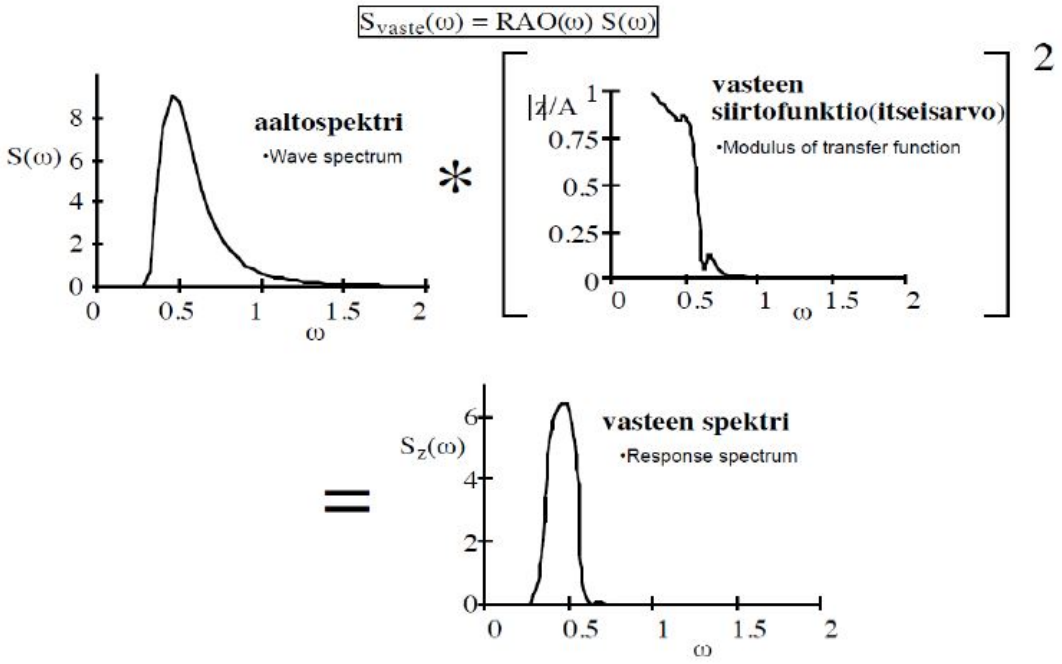

Figure 2.5. RAO Transfer Function. Source: [7].

Essentially, Figure 2.5 shows that one can begin by determining a wave spectrum of interest. The RAO is then multiplied by this wave spectrum and the result is the response of the vessel. Commonly, the response is desired in terms of pitch, roll, and yaw for vessels on the surface.

In Chapter 5 of this thesis, the basic premise for RAO used in linear seakeeping theory will be applied to forces and moments on shallowly submerged vessels. Specifically, an operator can be created which acts as a transfer function and allows rapid conversion from the amplitude and frequency of the wave into forces and moments on the shallowly submerged vessel.

2.5 Previous and Concurrent Research at NPS

Jones [8] created a computation fluid dynamics model in order to predict the forces and moments on submerged objects. Jones then compared the simulated results to experimentally produced data. The conclusion reached is that the forces and moments from the computational fluid dynamics model closely resemble the experimental data for wavelengths less than 1.4 times the model length. For longer wavelengths the simulation over predicted the loads. It is believed that further temporal refinement and lateral grid refinement could improve the predictions [8]. That is to say that for single regular waves, it is possible to closely predict the loads that would be exerted on a shallowly submerged vessel if the wave parameters are known.

Work by Turner et al. [9] utilized the aforementioned equations from Cummins to calculate a closed form analytical solution of the drag and vertical forces as well as pitching moment for a shallowly submerged vessel of a specific canonical shape. A model was then placed in the tow tank and the three parameters were measured at varying wavelengths and two different depths. The two depths analyzed were H^* of one and two. A graphical representation of the results is shown in Figures 2.6 – 2.8.

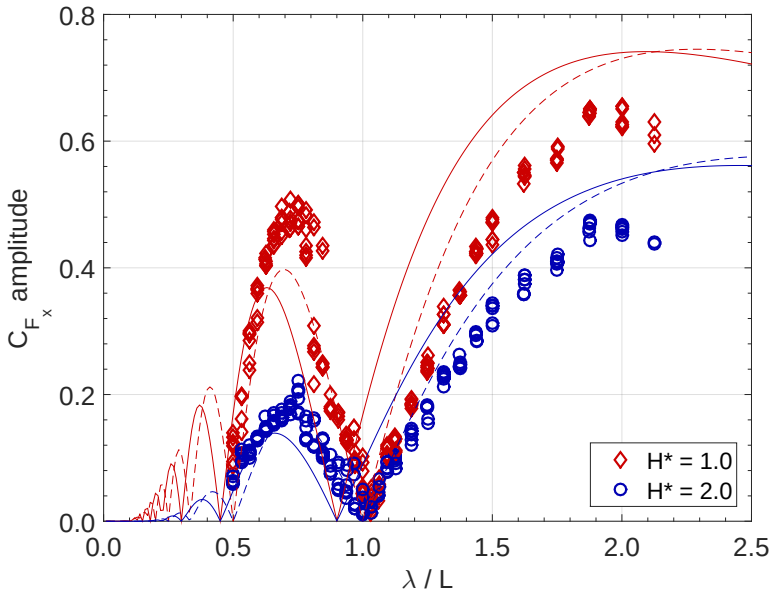

Figure 2.6. Non-dimensional Drag Force - Experimental vs. Theoretical Results. Source: [9].

The results of the experiment show that for the deeper submerged case, the analytic solutions

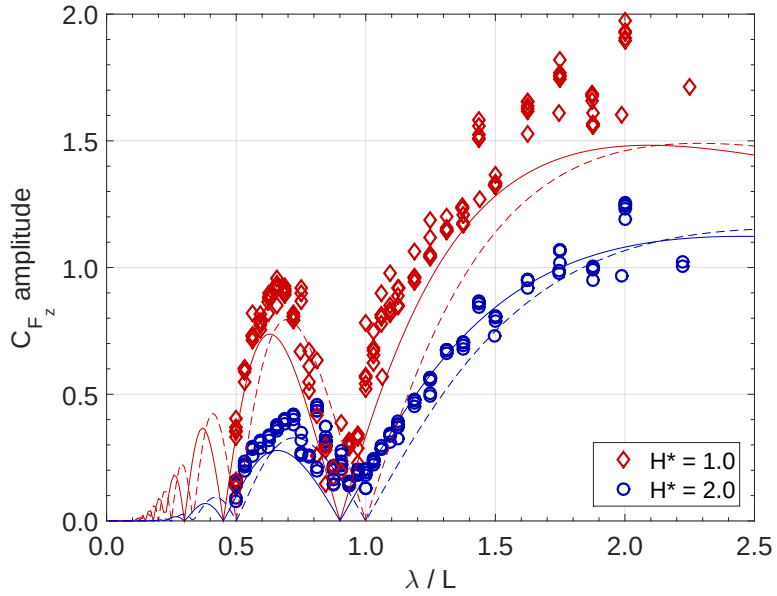

Figure 2.7. Non-dimensional Vertical Force - Experimental vs. Theoretical Results. Source: [9].

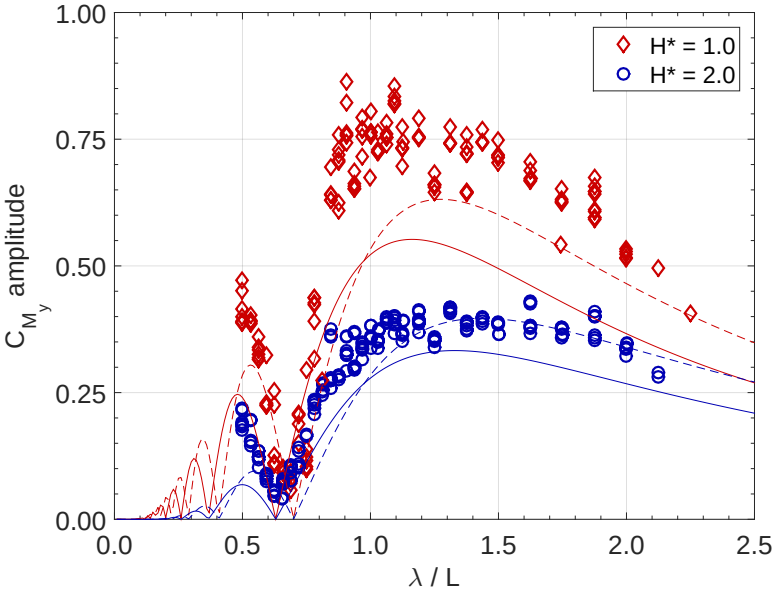

Figure 2.8. Non-dimensional Pitching Moment - Experimental vs. Theoretical Results. Source: [9].

do a reasonable job of predicting the loads. For the shallower submerged case however, the agreement between the two is much worse. Turner et al. attributes this to "the alteration of the wave profile as it passes over the body in such cases that it deviates from a regular wave

profile that the theory requires" [9].

Lieutenant Travis Turner is completing work on a concurrent thesis titled "Analyzing UUV Hull Cross-Sections for Minimizing Wave Loads When Operating Near Surface." Specifically, the study aims to measure the loads due to single regular waves on four different geometries of UUV. The geometries studied are rectangular (oriented vertical and horizontal), square, and circular. Each geometry will be studied at different shallow depths and wavelengths of single regular waves.

CHAPTER 3:
Experimental Setup

3.1 Description of Wavemaker

The experiments were conducted using the wavemaking tow tank located at the Naval Postgraduate School Hydrodynamics Laboratory. The tank is approximately three feet wide by four feet deep and a total length of 36 feet. The tank contains a plexiglass sidewall to allow for visual observation during testing. There is a movable carriage plate mounted above the tank which is affixed to rails which span the length of the tank. Because this experiment was conducted utilizing a stationary underwater model, the model was actually attached to a stationary frame that surrounded the tank and isolated the model from the noise and vibration of the wave maker. In order to produce the desired waves, a wavemaker at the near end of the tank was used. The wavemaker is a vertically movable wedge with a 35-degree interior angle that is approximately two feet in height and nearly the width of the tank.

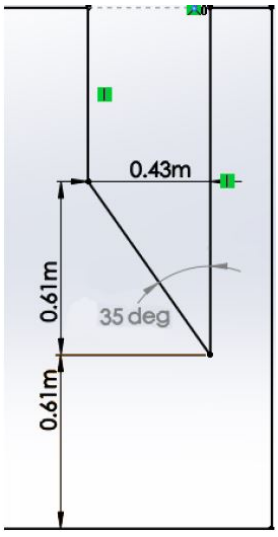

Figure 3.1. Wedge Geometry. Source: [8]

The wedge creates waves by moving up and down vertically. The wedge is affixed to a support frame made of pre-fabricated 80/20 t-slotted aluminum. The oscillatory motion

of the wedge is provided from an electric motor and linear actuator assembly. The wedge frame slides in between two bearing rollers which ensures the motion of the wedge is kept vertical. The maximum vertical travel of the wedge assembly is approximately 3.5 inches both up and down for a total of 7 inches of travel.

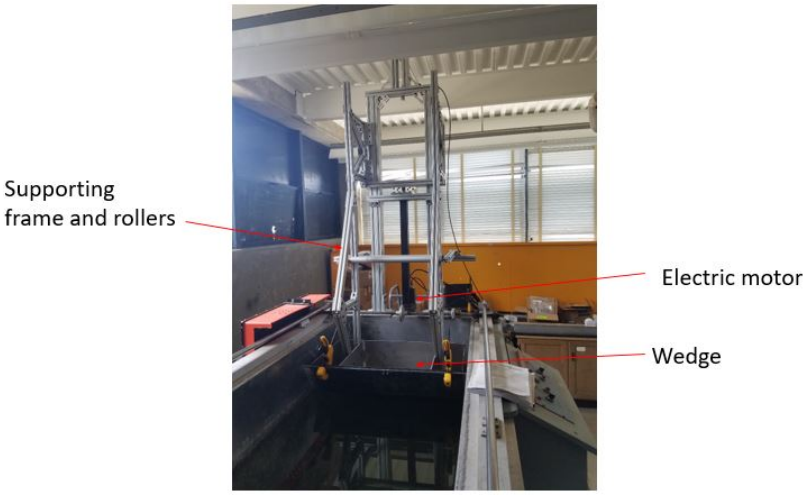

Figure 3.2. Wedge Assembly

The motion of the wedge is primarily controlled by three systems. These systems include an electric motor, control system, and linear actuator assembly. The basic design is straight forward as the control system receives inputs of motion amplitude, frequency, and phase from the user and then translates these inputs into commands for the motor controller. This signal is then received by the electric motor which drives the linear actuator assembly to oscillate the wedge vertically. The electric motor used is a MOOG - Animatics MT Motor (SM34165MT). The motor controller is a Modusystems Pulse/Dir motor conotroller (MAC-2TC). The linear actuator is an E-drive L-TAC LS long stroke ball screw actuator (LS204-24).

At the opposite end of the tank from the wave-making wedge is an energy absorbing beach made of two perforated acrylic sheets. The sheets contain 3/8-inch diameter holes drilled across the surface. The beach is affixed at an angle of approximately 12 degrees of incline for maximum energy absorption. The beach helps to ensure that only a small amount of energy is reflected back from the far end of the tank.

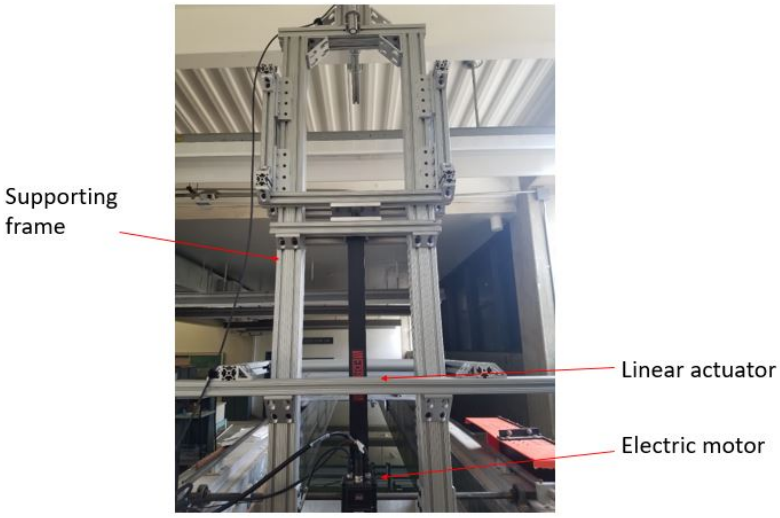

Figure 3.3. Backside of Wedge

3.2 Model and Test Setup

The model used was a 4.5-inch diameter cylindrical tube with hemispheric end caps placed on each end. The cylindrical body of the model was made of 1/8-inch thick extruded aluminum. The end caps were made of polycarbonate and made using a 3D printer located at the Naval Postgraduate School.

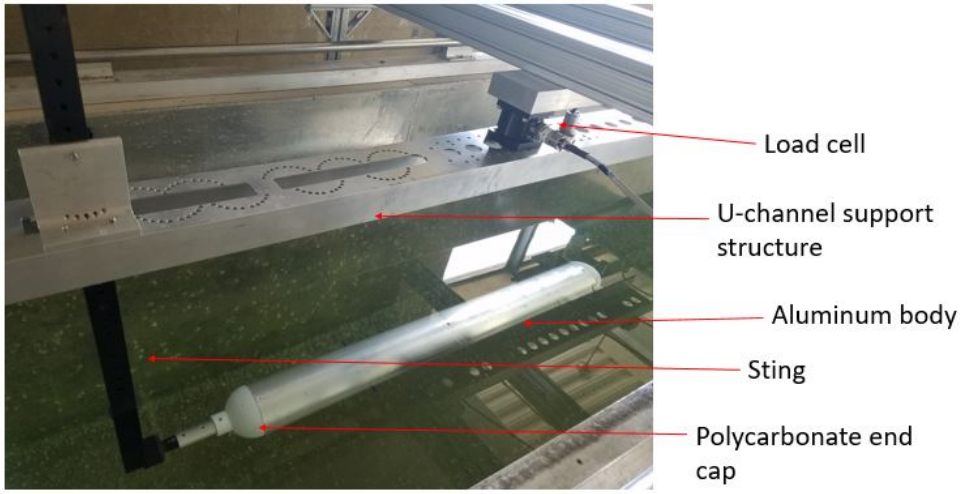

Figure 3.4. Model

The model was 45 inches in length to achieve a length to diameter ratio of 10. The

model contains a series of 1/8-inch bleed holes which allow the structure to be filled with water when submerged and prevent air from being trapped in the body. A sting assembly containing a vertical 1.0- by 1.5-inch rectangular aluminum bar approximately 46 inches long with pre-drilled holes spaced one inch apart serves to affix the model in place. Attached to the vertical bar is a horizontal 1.25-inch outer diameter aluminum tube with a thickness of 1/8-inches which slides inside the model and attaches with screws. This entire sting assembly allows the model to be moved to varying depths according to experimental needs. The sting assembly is attached to a U-channel via 90-degree angle brackets. These angle brackets can be used to adjust the pitch of the model, but again for the purposes of this experiment the model is kept at zero degrees of pitch. The load cell is also mounted to the top of the U-channel which is then connected to an aluminum 80/20 structure to provide support and minimize vibrations.

3.3 Instrumentation

The instrumentation used in this experiment consists of two major components. The first is a single three-axis AMTI MC3A load cell. The load cell is used to measure the forces and moments, each in three dimensions. Thus, there are six channels on the load cell that can be managed independently. For each channel, the voltage and gain were adjusted to provide the highest resolution possible for the predicted measurement range. The load cell is connected to a Gen5 signal amplifier which allows for the management of the individual channels and output voltages. The load cell settings used for this experiment are shown in Table 3.1. With these settings, the load cell was verified to be accurate within 0.25 pounds for the forces and 2 inch-pounds for the moments under an in-situ, but static, condition. This was verified through an in-situ load verification test conducted by placing known weights on the model while it was mounted on the sting and submerged such that the top of the hull was just at the calm water surface. The verification test was conducted by Lieutenant Travis Turner.

The other major component of instrumentation is a set of four Senix ToughSonic 14 ultrasonic probes. These probes are mounted along the U-channel at the centerline of the tank and at various longitudinal distances relative to the model origin. The probes measure real-time wave heights and allow for the construction of a wave time history during testing. The wave probes were placed approximately 9 inches above the calm water mean level and

	Channel		
Parameter	F_x	F_z	M_y
Excitation Voltage	10 (V)	10 (V)	10 (V)
Gain	4000	4000	500
Analog Sensitivity	± 20.69 (lbs)	± 81.51 (lbs)	± 118.18 (lbs)

Table 3.1. Load Cell Settings

configured to measure from 5 to 15 inches from the sensor.

Both the load cell and wave probes were connected to a National Instruments data acquisition board (USB-6363). The data acquisition board was connected to a computer via Universal Serial Bus (USB) cable to allow for real time collection of data.

3.4 Wave Probe Calibration Verification

To ensure accuracy of the experimental data, the wave probes were tested to verify the manufacturer's calibration. As previously mentioned, the wave probes were configured to measure distances from 5 to 15 inches from the sensor using Senix software. The wave probes are capable of producing a signal from zero to ten volts. Thus a gain of -1 is used for this experiment. The value of one for the gain is intuitive as it is simply defined by the ratio of the measurement range to the output voltage range. In this case, the measurement range and voltage range are each ten, leading to the value of one. However, the negative sign may be a bit less intuitive and is a result of being in different frames of reference. If we assume a calm water of eight inches below the probe, this will result in a zero file of 3 volts. During a run, a two inch amplitude wave crest will be six inches away from the probe. The probe will return a voltage of one volt. After removing the zero value this will result in a value of -2 volts. Applying the gain of 1-inch per volt results in a wave crest height of -2 inches. However since this is the crest of the wave we prefer the value to be positive, hence the negative sign associated with the gain. The same logic applies to a trough which is ten inches away from the probe so it returns a reading of five volts. After removing the zero value, the result is 2 volts. Applying the gain of 1 inch per volt returns a trough of 2 inches which we again would prefer have the opposite sign. Therefore, a gain of -1 inches per volt is used.

The calibration check for each probe was conducted by adjusting the distance from the probes to the water from 5 to 13 inches in 1.0-inch increments. All four probes were checked simultaneously using a thin rectangular bar which contained four holes for mounting the probes. The bar was slightly less than 36 inches in length to allow it to fit within the width of the tank. The custom wave probe bar was then attached to a vertical post via a custom made 90-degree elbow and mounting bracket. The vertical post contained holes at one inch increments which allowed for movement of the probes vertically by unscrewing the 90-degree elbow and reinstalling it at the new height. At each one inch height iteration, a 60-second data set was taken. This process was completed three times for the range of values. The data was then plotted in Excel and a linear regression was performed for each individual probe to verify the manufacturer's calibration. The results are shown in Figure 3.5. The y-axis in the plots is labeled as the height above the baseline, which in this case is five inches. At a height of five inches above the water, it is expected that the probes return a voltage of zero Volts. As one can see, the results were satisfactory. The slope of the gain for each probe is very near one.

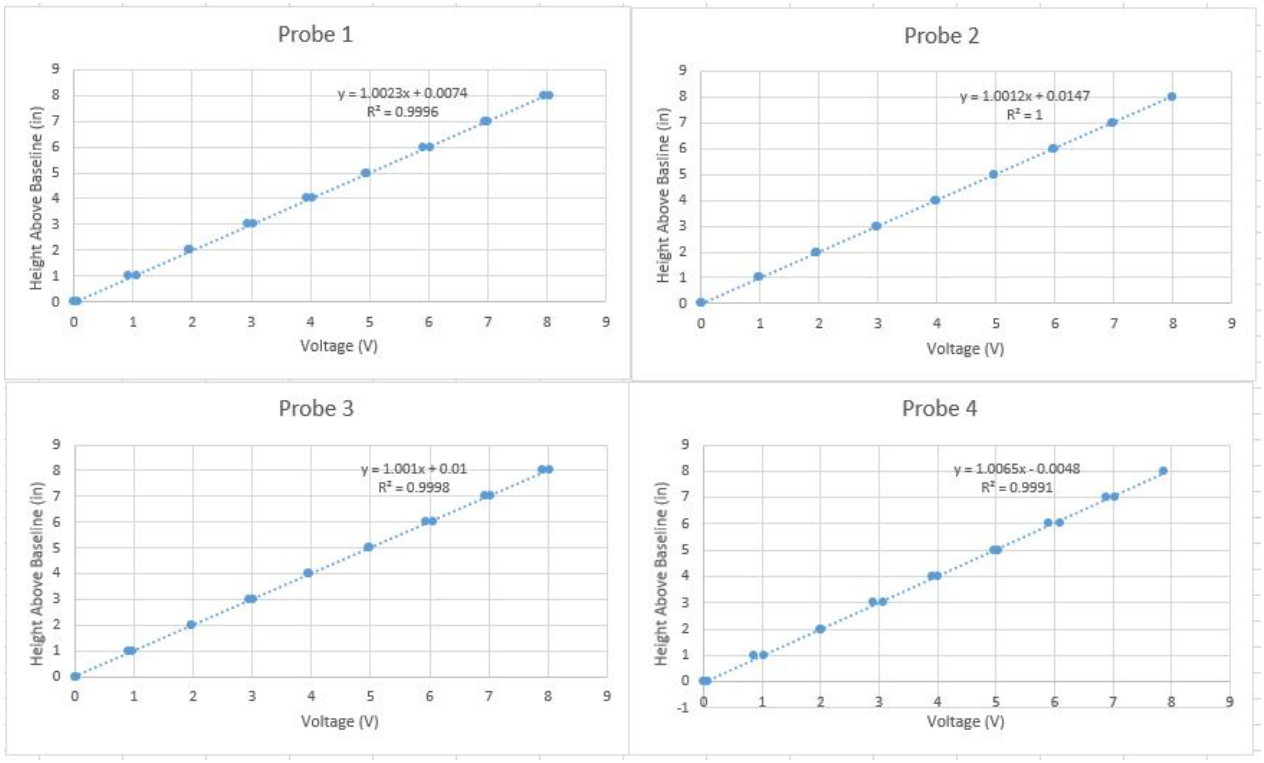

Figure 3.5. Probe Calibration Results

CHAPTER 4:
Data Collection and Reduction

4.1 Collection Process and Reduction

Data was collected from the wave probes and load cell via the data acquisition board to a computer which is connected via USB cable. A custom MATLAB script was written to collect the data and plot channels of interest in real time. The raw data was captured into .dat files for later use in data reduction. Each run was conducted for 60 seconds at 50 Hertz (Hz) for a total of 3,000 data points per channel per run.

The raw data in the .dat file for each run is then ready for data reduction. Before each data collection session, a calm water zero file is taken. The mean of each channel in the zero file is calculated and this value is removed from the corresponding channel in the run file. From here, the gain of each sensor can be applied to convert the voltage reading into physical units. These units are inches for the wave height, pounds for the forces, and inch-pounds for the moments. This was achieved using a custom MATLAB script which also serves to remove erroneous readings from the wave probes due to excessively steep waves. After the data was properly cleaned, the wave elevation and load time histories were ready to be analyzed.

4.2 Sine Wave Amplitude and Phase Identification

For a complex irregular time history signal, the amplitude and phase of each underlying component can be determined. The process of determining each amplitude and phase for n number of underlying waves is done using a least squares curve fit equation of the following general form.

$$f(x,t) = A_1 \sin(k_1 x - \omega_1 t) + B_1 \cos(k_1 x - \omega_1 t) + A_2 \sin(k_2 x - \omega_2 t) + B_2 \cos(k_2 x - \omega_2 t) +$$
$$A_3 \sin(k_3 x - \omega_3 t) + B_3 \cos(k_3 x - \omega_3 t) + A_4 \sin(k_4 x - \omega_4 t) + B_4 \cos(k_4 x - \omega_4 t) + ... + C$$

The equation shown is written for four waves, but the equation can be written for any number of wave components in the complex signal. In order to calculate the least squares curve fit,

a custom MATLAB script was written which reads in the cleaned data from a designated .dat file. Furthermore, trigonometric identities allow for the sine and cosine components of a wave to be written as a single sine with a phase as follows.

$$\alpha \sin(\omega t + \phi) = \beta \sin(\omega t) + \gamma \cos(\omega t) \tag{4.1}$$

The amplitude of each single regular wave can be written as simply

$$\alpha = \sqrt{\beta^2 + \gamma^2}. \tag{4.2}$$

The phase shift of each wave can be written as simply

$$\phi = \tan^{-1}(\beta/\gamma). \tag{4.3}$$

Thus, to determine the wave amplitude and phase of each single regular wave that makes up the complex wave form, the MATLAB script begins by using a least squares curve fit to calculate an optimal A and B value for each wave frequency provided. Then using basic trigonometry, the sine and cosine terms can be combined into a single sine expression. Given this information, it is possible to calculate the wave amplitude and phase of a component wave.

4.3 Wave Environment Determination

As previously discussed, the wave probes measure a voltage as a function of time. The voltage is then converted to a distance based on the gain which the sensor is set to. For this experiment, a gain of -1 with a distance of 5 to 15 inches from the sensors was used.

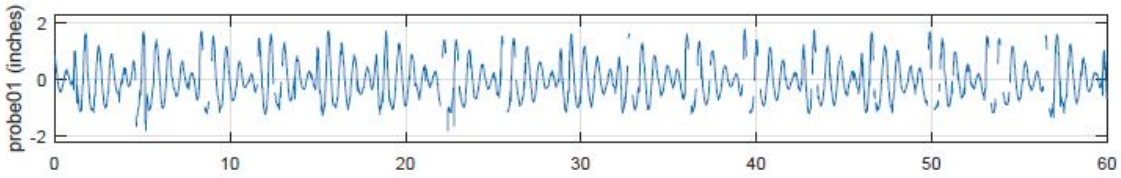

Figure 4.1. Experimental Wave Time History

Figure 4.1 shows an example wave time history for a complex wave environment made up of two single regular waves. The waves used for this example were a 0.5-inch amplitude

1.52 Hz wave and a 1.0-inch amplitude 1.227 Hz wave. It is also important to note that the wave time history shown is after the data has been cleaned of outliers as described in Section 4.1. The underlying frequencies of interest in the wave system are known since they correspond to the wedge driving frequencies. Therefore, these frequencies were provided to the MATLAB curve-fitting routine described in Section 4.2 and the amplitude and phase for each of the waves was calculated.

4.4 Vehicle Load Amplitude and Phase Estimation

Since the vehicle load time history signal is also a complex irregular signal that is a scaled and phase shifted version of the wave elevation time history, the amplitude and phase estimation is calculated similar to the wave amplitude and phase identification in Section 4.2. In order to decompose the complex forces and moments into their simpler components, the same MATLAB curve-fitting function was utilized.

It is also important to note that the measured pitching moment at the load cell origin is not all due to the pitch moment at the vessel origin, which is where we will ultimately report the moments about. Therefore, the moments must be moved using the following equation

$$M_f = M_i + \vec{r} x \vec{F}. \tag{4.4}$$

This will remove the drag induced pitching moment measured at the load cell origin. For this experiment, the measured pitch moment is a sum of the moment induced due to the drag force as well as the pitch moment on the vessel. It is also important to note that the sting contributes to all the forces and moments as well. In order to determine only the hydrodynamic loads on the body these sting effects would need to be removed. Since we are only interested in seeing if the individual regular wave results are consistent with complex irregular wave results that contain those regular waves, the effects of the sting were not removed. It is reasonable to believe that if linear superposition is valid with the sting included in the data, it would also be valid with the sting data removed.

4.5 Importance of Wave Frequency Sums and Differences

In combining multiple single regular waves, interactions between the different waves can give rise to some non-linear effects. Specifically, non-linear wave theory shows that at the

wave frequency sums and differences, it is possible for energy to be present due to these special interactions. This is an important effect as one would expect only to detect energy at the frequencies of the single regular waves. In order to detect if this non-linearity is present, graphs in the frequency spectrum will be analyzed. In a truly linear system with no interactions, energy peaks would only be seen at the frequencies of the component waves. If single regular wave load RAOs are valid, and force can be predicted by only knowing the amplitude and frequency of the underlying wave components, then it follows that the force as a result of the non-linear interactions could also be calculated and included.

4.6 Test Matrix

To help organize the data collection process, a test matrix was created. This test matrix takes inputs from the user on desired wave height, length of the model, maximum wavelength, and depth of the water. It then applies the wave to wedge transfer function and calculates the frequency of the desired wave as well as the wedge ampltiude command for each desired frequency.

An abbreviated example of the test matrix is shown in Figure 4.2. The actual test matrix used covers a range of λ/L values from 0.5 to 2. These values were chosen because they are both realistic for a real-world seaway as well as for inherent wavemaker limitations.

4.7 RAOs from Single Wave Results

It is also desirable to reduce the four different amplitude single regular wave graphs for the forces and moments presented in Chapter 5 into a single dimensionless graph for each load parameter. By non-dimensionalizing the drag force, vertical force, and pitching moment, the data should collapse to single curves and these loads could be predicted by only knowing the wave height, frequency, and properties of the submerged body. In order to non-dimensionalize the forces and moments, coefficients are created for each and Equations 2.1, 2.2, and 2.3 are simplified. The general equation for the force coefficient is:

$$C_f = \frac{F}{\rho g A_o h} \tag{4.5}$$

water depth =	3	(ft)						a_wave / a_wedge = Af^2+Bf+C		
max wave lenth =	6	(ft)						A =	-0.225376	
Desired Wave Height =	1	(inches)						B =	1.5621619	
model length =	45	(inches)						C =	-0.525838	
				goal seek to 1 by changing period						
	desired	required								ITERATED
	lambda / L	wave length	steepnes	goal seek fn	period	freq	wedge actua	wedge CMD	wedge CMD	
	(---)	(ft)	(---)		(sec)	(Hz)	(in)	(mm)	(mm)	
1	0.5000	1.875	22.5	1.00000008	0.6051152	1.653	0.34716136	17.636		
2	0.5313	1.992	23.9063	1.00000008	0.62373847	1.603	0.35730145	18.151		
3	0.5625	2.109	25.3125	1.00000008	0.6418216	1.558	0.3673775	18.663		
4	0.5938	2.227	26.7188	1.00000008	0.65940903	1.517	0.37739373	19.172		
5	0.6250	2.344	28.125	1.00000008	0.67653943	1.478	0.38735461	19.678		
6	0.6563	2.461	29.5313	1.00000008	0.6932467	1.442	0.39726473	20.181		
7	0.6875	2.578	30.9375	1.00000008	0.70956078	1.409	0.40712859	20.682		
8	0.7188	2.695	32.3438	1.00000008	0.72550825	1.378	0.41695063	21.181		
9	0.7500	2.813	33.75	1.00000008	0.74111285	1.349	0.42673513	21.678		
10	0.7813	2.930	35.1563	1.00000008	0.75639595	1.322	0.4364862	22.173		
11	0.8125	3.047	36.5625	1.00000008	0.77137681	1.296	0.4462078	22.667		
12	0.8438	3.164	37.9688	1.00000008	0.78607296	1.272	0.45590376	23.160		
13	0.8750	3.281	39.375	1.00000008	0.80050036	1.249	0.46557774	23.651		
14	0.9063	3.398	40.7813	1.00000008	0.81467366	1.227	0.4752333	24.142		
15	0.9375	3.516	42.1875	1.00000008	0.82860636	1.207	0.48487387	24.632		
16	0.9688	3.633	43.5938	1.00000008	0.84231093	1.187	0.4945028	25.121		
17	1.0000	3.750	45	1.00000008	0.85579896	1.168	0.50412337	25.609		

Figure 4.2. Sample Test Matrix

And for the moment the coefficient is:

$$C_m = \frac{M}{\rho g A_o L h} \tag{4.6}$$

Both equations satisfy the idea of the RAO since they represent a force or moment response per unit wave height. These equations will provide the basis for producing dimensionless coefficient versus non-dimensional wavelength curves for the drag force, vertical force, and pitching moment. Then a least squares regression will be calculated to form a line of best fit for each curve. This curve fit will be calculated by solving for the coefficients in Equations 2.4 – 2.6 after non-dimensionalizing the data.

4.8 Force Predictions Using RAO Transfer Functions

In the results section, this thesis will demonstrate how to produce a RAO transfer function which allows for the rapid conversion from the wave amplitude and frequency to predicted forces and moments. For the purposes of this experiment, this will allow for the prediction

of force and moment time histories by knowing the wave amplitude, frequency, and the RAO transfer function.

The RAO transfer function that will be used is the non-dimensional force and moment coefficients derived in Equations 4.5 and 4.6. The vertical force due to a single regular wave can then be calculated as follows

$$F_{z,i} = -C_{fz}\rho g A_o 2w_{a,i}\sin(\omega_i t + \theta_t). \tag{4.7}$$

Where C_{fz} is the RAO evaluated at the ω_i frequency and has the functional form of Equation 2.2 and θ_i is the sum of the phase angle of the load of interest relative to the incoming wave plus the specific phase of the wave of interest. Linear superposition then says that the total vertical force is equal to the sum of all the individual single regular wave forces. Thus the vertical force can simply be defined as:

$$F_z(total) = \sum_{i=1}^{n} -C_{fz}\rho g A_o 2w_{a,i}\sin(\omega_i t + \theta_t) \tag{4.8}$$

This process can also be repeated quite easily for the drag force and pitching moment and the results are as follows:

$$F_x(total) = \sum_{i=1}^{n} -C_{fx}\rho g A_o 2w_{a,i}\cos(\omega_i t + \theta_t) \tag{4.9}$$

$$M_y(total) = \sum_{i=1}^{n} C_{my}\rho g A_o L 2w_{a,i}\cos(\omega_i t + \theta_t) \tag{4.10}$$

The effectiveness of the RAO approach is tested in Chapter 5 when the transfer function is applied to predict a vertical force time history. This will then be compared to experimental data.

CHAPTER 5:
Data Results

5.1 Single Regular Wave Results

The first portion of the experiment begins with creating single regular waves using the wavemaker. The wave amplitudes studied are 0.25, 0.50, 0.75 and 1.0 inches. The calm water centerline depth of the shallowly submerged vessel is twice its diameter. In this case this diameter is 4.5-inches, leading to a centerline submergence of nine inches. The λ/L values are varied from 0.5 to 2 in small intervals and this process is repeated four times for each wave amplitude. For each iteration of λ/L values, there are 30 data points and because each is replicated four times, there are 120 data points for each wave amplitude. As aforementioned, the parameters of concern are drag force, vertical force, and pitching moment. The results for the drag force are shown below:

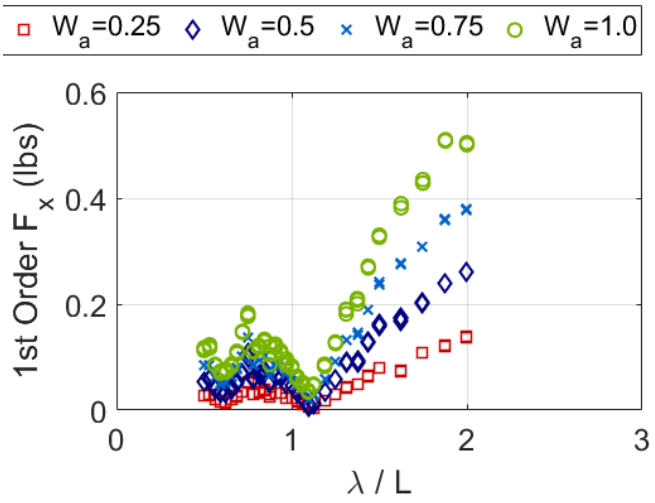

Figure 5.1. Single Regular Wave Data - Drag Force

The results for the drag force are close to what one would expect based on Equation 2.2. The drag force increases nearly linear in terms of wave height. It is also quite obvious that the graph can be broken down into two distinct ranges. These ranges are for λ/L values less than one and greater than one. For λ/L values greater than one, much larger drag forces

are observed and these forces tend to increase under longer wavelength waves. Again this agrees with Equation 2.2. For λ/L values less than one, we see generally lower drag force values under 0.15 lbs. The drag force values tend to increase from a λ/L of about 0.5 to 0.8, before decreasing from 0.8 to approximately 1.1. For the results of overall drag force, the drag force exerted on the sting has not been removed from the data. It is believed that this would have a greater relative effect on λ/L values less than one where overall forces tend to be reduced.

The next step is to use a least-squares regression to create a curve fit for each curve shown in Figure 5.1. This is done using a custom MATLAB script and fitting to a function of the form of Equation 2.4. This curve fit function is a reduced form of Equation 2.1 where the coefficients of A, B, and C represent the associated group of variables from the equation. The results for the drag force coefficient curve fitting are shown in Table 5.1. These curve fit coefficients will be used later during the multiple wave construction and decomposition to represent single regular wave results.

Fx Curve Fit Coefficients				
	Amplitude (inches)			
Coefficient	0.25	0.5	0.75	1
A	-0.27863	-0.54002	-0.75832	-1.13748
B	3.487168	3.487168	3.455752	3.424336
C	-1.50796	-1.48283	-1.3823	-1.54566

Table 5.1. Drag Force Curve Fit Coefficients

The results for single wave vertical forces are shown in Figure 5.2. The results for the vertical force look similar to those of the drag force. There are once again two distinct regions on the graph. These ranges are for λ/L values less than one and greater than one. We also observe the similar linear increase of vertical force with wave height. Another takeaway is that the vertical force is larger than the drag force. The Cummins equations predict that the vertical force should be approximately twice the drag force. The Cummins predictions prove to be close in this case. For example, for a wave amplitude of 0.75-inches and λ/L of 2, the vertical force is about 0.95 lbs. Under the same conditions, the drag force is approximately 0.4 lbs.

Similar to what was done for the drag force, the next step is create a curve fit function for each wave amplitude shown in Figure 5.2. Again a least-squares regression is used to fit a

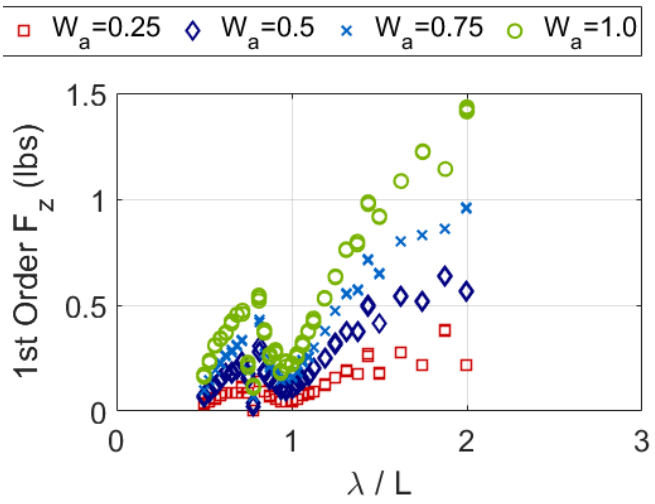

Figure 5.2. Single Regular Wave Data - Vertical Force

function of the form of Equation 2.5. This curve fit equation is the reduced form of Equation 2.2 where the coefficients A, B, and C are used to denote a combination of variables. A summary of the curve fit coefficients is displayed in Table 5.2.

Fz Curve Fit Coefficients				
	Amplitude (inches)			
Coefficient	0.25	0.5	0.75	1
A	-0.49406	-1.02833	-1.51664	-2.1141
B	2.984513	2.984513	3.015929	2.984513
C	-1.03044	-1.04301	-0.98018	-1.01788

Table 5.2. Vertical Force Curve Fit Coefficients

The last factor examined for the single regular waves is the pitching moment. Much like the case for the drag force, it is important to note that the pitching moment exerted on the sting has not been removed from the data. That is to say that the moments shown are actually a combination of the moment exerted on the body as well as the sting. The sting moment data has not been removed primarily due to a lack of time afforded to complete the study. The pitch moment has, however, been moved from the load cell origin to the model origin. The results for the pitching moment of four different amplitude single regular waves are shown in Figure 5.3.

One of the interesting results is that there are still two distinct regions on the graph, but

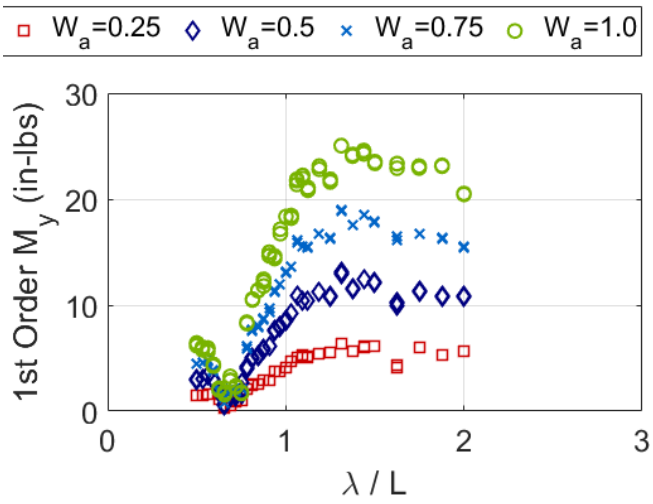

Figure 5.3. Single Regular Wave Data - Pitching Moment

the regions have shifted slightly. For example, for a 0.75-inch amplitude wave, the pitching moment is about five inch-lbs at a λ/L of 0.5. The pitching moment steadily decreases down to near zero at a λ/L of about 0.75 before climbing again to about 16 inch-lbs at a λ/L of two. This is slightly different from the drag and vertical forces where the zero point was observed at a λ/L of about one. The other important thing to note is the magnitude of the pitching moment. For 1.0-inch amplitude waves at long wavelengths, pitching moments of about 25 inch-lbs were observed.

Similar to what was done for the forces, the next step is create a curve fit function for each wave amplitude shown in Figure 5.3. Again, a least-squares regression is used to fit a function of the form of Equation 2.6. This curve fit equation is the reduced form of Equation 2.3 where the coefficients A, B, C, D and E are used to denote a combination of variables. A summary of the curve fit coefficients is displayed in Table 5.3. Once again, these curve fit coefficients will be used later during the multiple wave construction and deconstruction portions of this experiment.

5.2 Experimental RAOs from Single Regular Waves

As introduced in Section 4.7, it is possible to non-dimensionalize the data present in Figures 5.1, 5.2, and 5.3. This essentially means to collapse the data from the four different wave heights into a single data set by applying the force and moment coefficient equations shown

My Curve Fit Coefficients				
	Amplitude (inches)			
Coefficient	0.25	0.5	0.75	1
A	1.02861	2.009218	3.024112	2.6881
B	1.884956	1.727876	1.727876	0.942478
C	-1.5708	-1.5708	-1.5708	-0.7854
D	2.513274	2.670354	2.670354	3.612832
E	-1.88496	-1.88496	-1.88496	-1.00531

Table 5.3. Pitching Moment Curve Fit Coefficients

in Equations 4.5 and 4.6. This process is again completed using a custom MATLAB script to plot the non-dimensionalized data and then using a least-squares regression to produce a line of best fit.

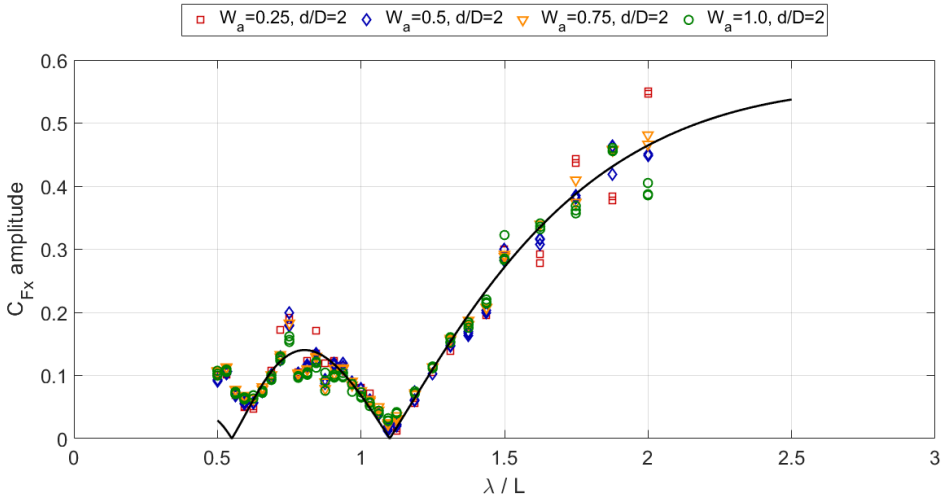

Figure 5.4. Non-dimensionalized Drag Force

Non-Dimensional Curve Fit Coefficients			
	Parameter		
Coefficient	Fx	Fz	My
A	-0.24	-0.54	0.31831
B	3.455752	3.015929	2.513274
C	-1.47027	-1.25664	-2.82743
D			2.513274
E			-2.38761

Table 5.4. Non-Dimensional Curve Fit Coefficients

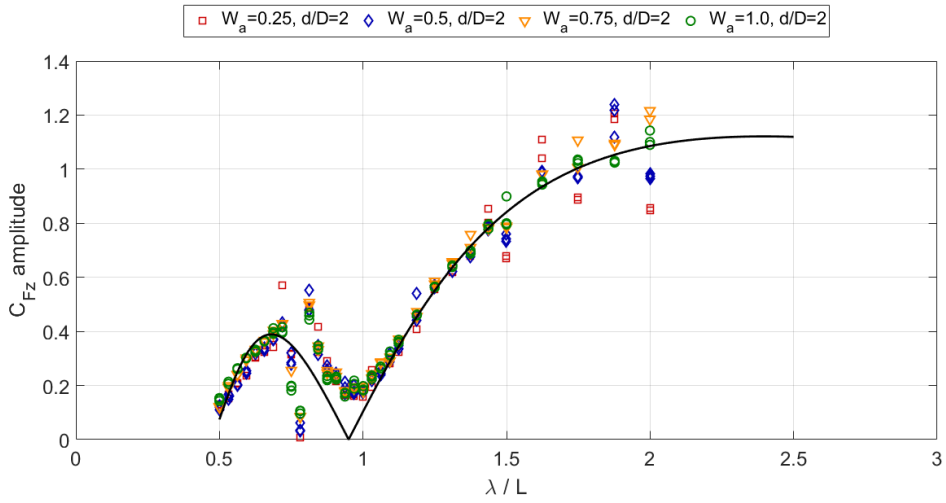

Figure 5.5. Non-dimensionalized Vertical Force

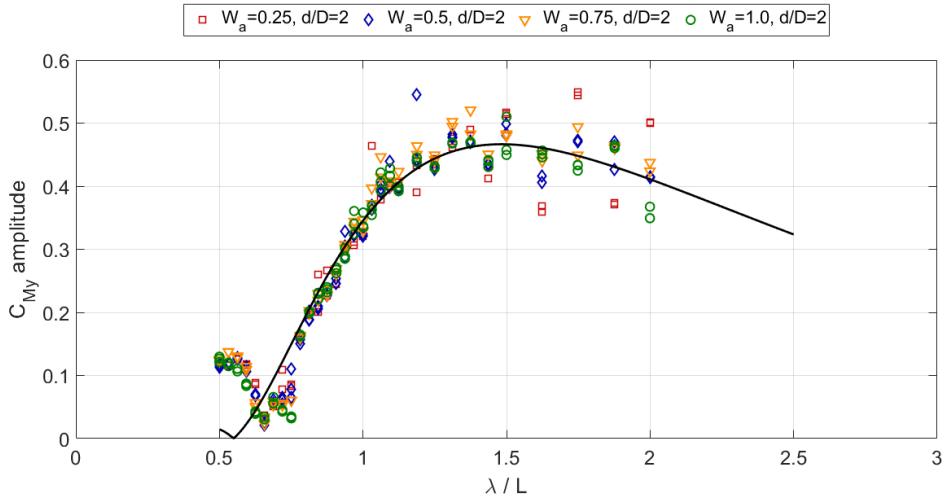

Figure 5.6. Non-dimensionalized Pitching Moment

Figures 5.4, 5.5, and 5.6 show the non-dimensionalized data along with the regression line for each parameter. A summary of non-dimensional curve fit coefficients is presented in Table 5.4. As one can see, the curve fits predict the experimental data pretty well. This is especially true for λ/L values greater than one. Also, there does appear to be a larger spread of data about the curve fit line as the λ/L values get very near two. Because the data appears to be spread quite evenly above and below the curve fit, this is attributed to random experimental uncertainty versus some non-linearity in the system.

The real novelty in these results is the calculation of the non-dimensional curve fit coefficients. Given this information, it is theoretically possible to calculate the forces and moments due to a single regular non-breaking wave of any amplitude and wavelength for a vessel with the same depth of submergence and geometrical properties. In order to do this, the coefficient force or moment value per unit wave amplitude is calculated based on the particular λ/L. The coefficient is then converted to a force by multiplying it by the denominator in Equation 4.5 or 4.6. This is important as it means a significant reduction in the time required to experimentally or analytically determine the forces and moments on a shallowly submerged vessel.

5.3 Irregular Two-Wave Seaway Deconstruction

An irregular two-wave seaway is created by combining a one-inch amplitude wave with a λ/L of 0.6 or 0.75, corresponding to a frequency of 1.52 Hz or 1.227 Hz, with a variety of half-inch amplitude waves. Specifically, the one-inch amplitude wave is held at constant frequency while the half-inch wave is varied from a λ/L of 0.5 to two with a different λ/L value being used for each run. There are 30 λ/L values tested between 0.5 and two. Each λ/L of 0.6 or 0.75 for the one-inch wave is tested once for a total of 60 runs. An experimental wave, vertical force, and pitching moment time history is shown in Figures 5.7, 5.8, and 5.9, respectively. The waves used for this sample run example were a 0.5-inch amplitude 1.52 Hz wave and a 1-inch amplitude 1.227 Hz wave. As one can see, the resultant wave elevation and force and moment time histories are irregular oscillating signals.

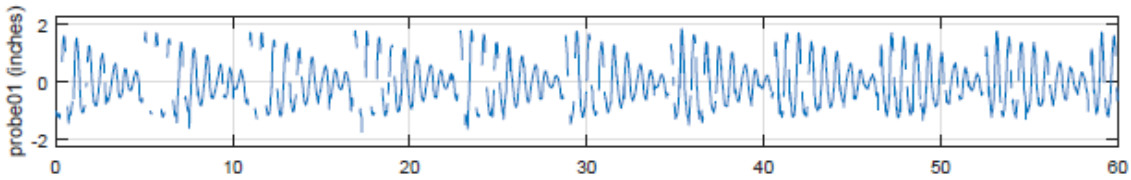

Figure 5.7. Experimental Wave Time History

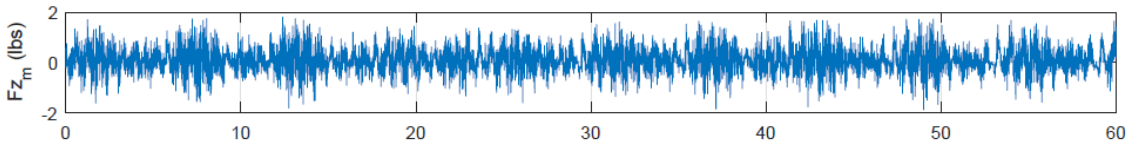

Figure 5.8. Experimental Vertical Force Time History

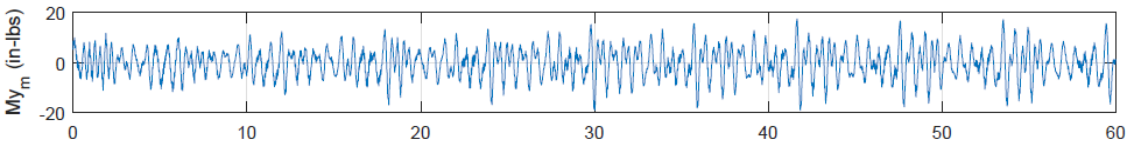

Figure 5.9. Experimental Pitching Moment Time History

Frequency spectrum plots can also be created. Plots displaying the wave height and vertical force in the frequency spectrum are shown in Figures 5.10 and 5.11, respectively. These results are from the same sample run example as Figures 5.7 – 5.9. Moving from left to right on Figure 5.10, the first red line represents the difference in frequency between the two component waves. The second and third red lines represent the frequency of each single wave. The fourth and last red line represents the sum of the two component frequencies. As expected, at each of these frequencies, there is a noticeable amount of energy contribution to wave height.

The plot displaying vertical force in the frequency spectrum has similar characteristics. Moving from left to right on Figure 5.11, the first red line represents the difference in frequency between the two component waves. The second and third red lines represent the frequency of each single wave. The fourth, fifth, and sixth red lines represent the sum of the two component frequencies, as well as twice the value of each component frequency. Once again there are noticeable peaks at each of these frequencies. These plots are helpful in visualizing the contribution of each underlying component frequency to the wave height, force, or moment of interest.

The forces and moments that result from each of the two underlying regular waves is estimated as described in Section 4.4. The forces and moments resulting from the 0.5-inch wave are then plotted against the single regular wave curve fit and the data is compared. The curve fits and predicted results are also shown for the wave which is held constant. The results are shown in Figures 5.12, 5.13, and 5.14. In each graph, the 0.5-inch single wave curve is represented by the dashed red line and the 1-inch single wave curve is represented by the dashed blue line. During testing, the underlying $\lambda/L = 0.6$ or 0.75, 1-inch wave was fixed while a 0.5-inch wave of various frequencies was tested across different runs. The 0.5-inch wave component contributions are shown in the figure as the red square data while the 1.0-inch wave component contributions are shown as the blue circle data. There are 30 red and blue data pairs corresponding to each run. Since the blue circle data was also at the

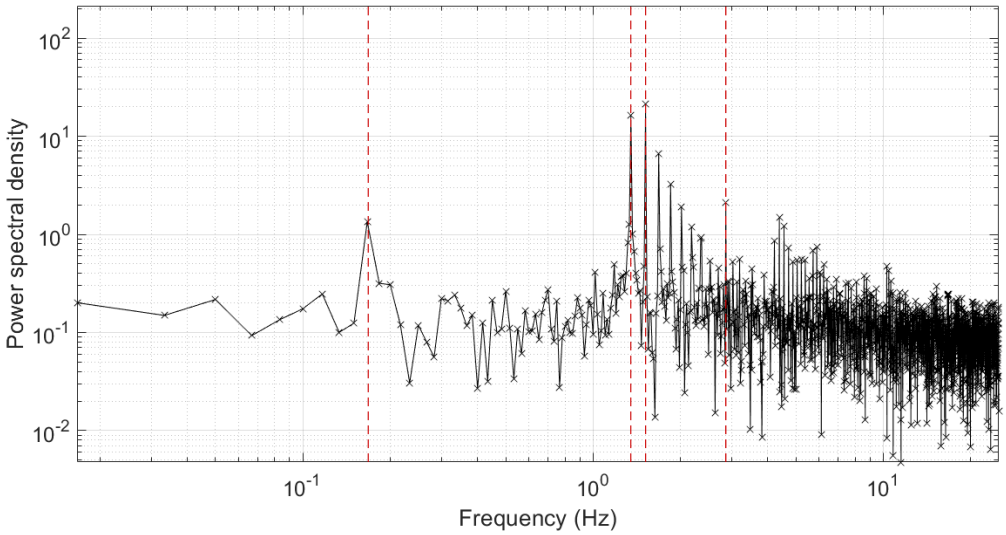

Figure 5.10. Wave Height in Frequency Spectrum

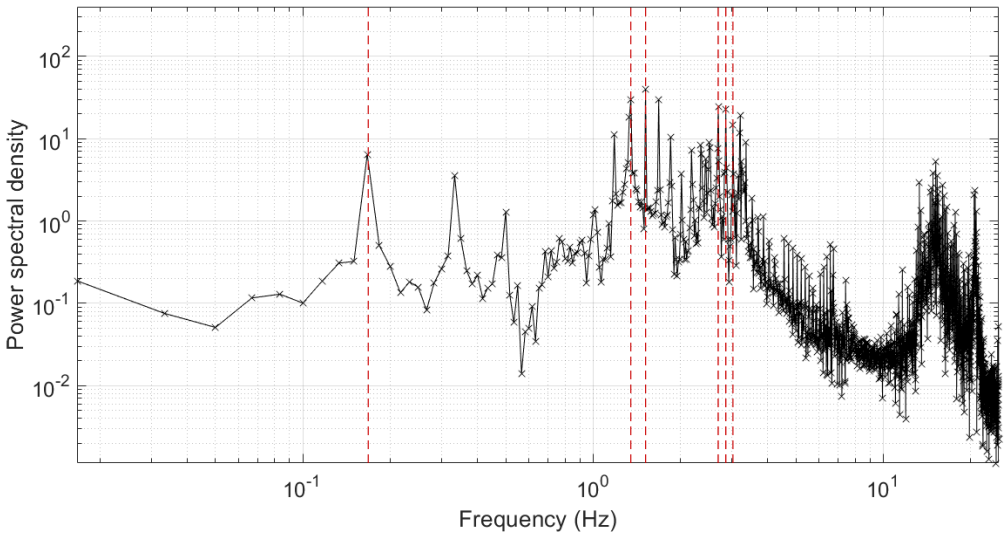

Figure 5.11. Vertical Force in Frequency Spectrum

same $\lambda/L = 0.6$ or 0.75, it is clustered on the figure. The 0.5-inch wave data corresponded to a different frequency each run so the red squares span the whole λ/L range.

Overall, the results appear to show that it is possible to use linear superposition to determine the forces and moments, especially for λ/L values greater than one. For the vertical force, the curve fit tends to over predict the results of the constant wave. For the pitch moment

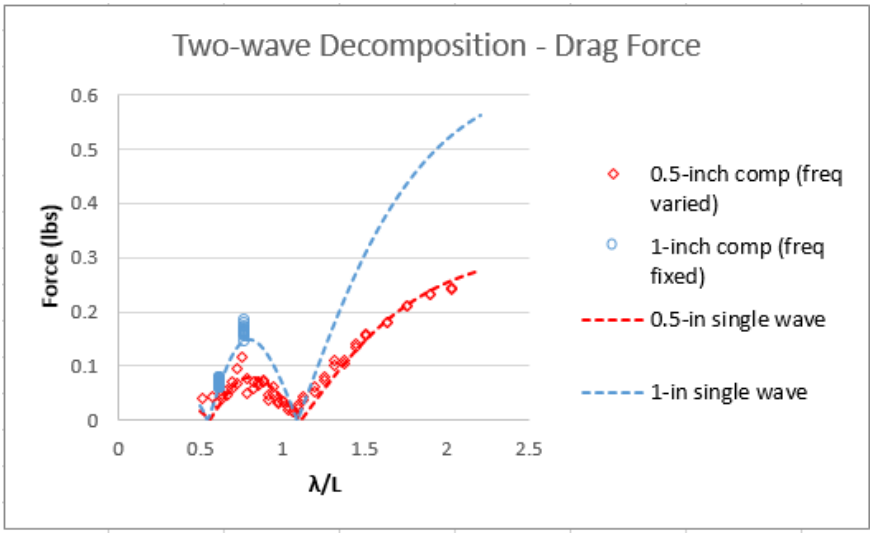

Figure 5.12. Irregular Two-Wave Drag Force

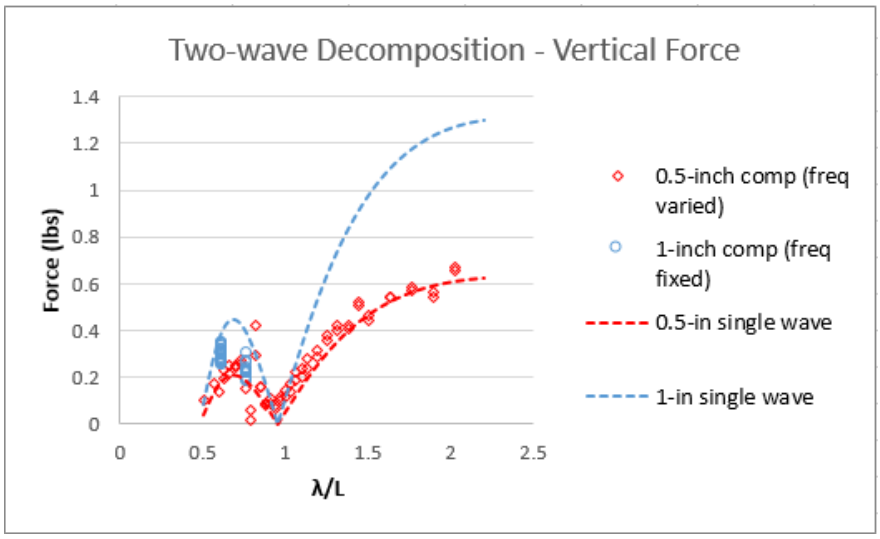

Figure 5.13. Irregular Two-Wave Vertical Force

results of the constant wave, it is difficult to gain any insight because the values are very near zero. The single wave curve fits do appear to under predict the pitching moment by a slight amount from λ/L values of about 0.7 to 1.4. The curve fits then appear to slightly over predict the pitching moment for λ/L values greater than about 1.5. There is a measurement uncertainty of about 2 in-lbs in the moment. On top of that, there is an uncertainty caused by moving the moment from the load cell origin to the model origin. With that in mind, the experimental results agree with the regular wave curve within the uncertainty of the

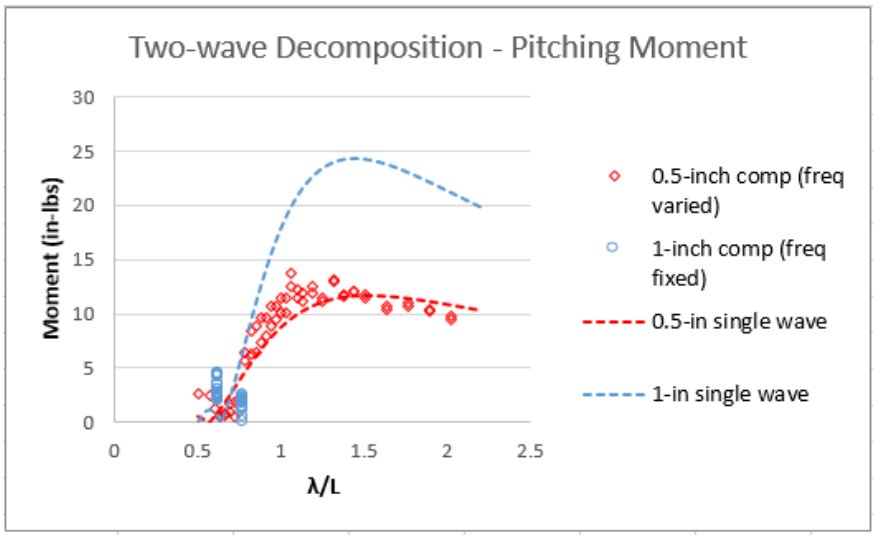

Figure 5.14. Irregular Two-Wave Pitching Moment

data. Still, there are some irregularities displayed when the two λ/L values are close to one another in each of the three graphs. In each case these irregularities occur when the two-wave data nears a λ/L of 0.7. This is primarily due to the difficulty in resolving two frequencies which are so close together with the given decomposition methods and equipment.

5.4 Irregular Three-Wave Seaway Deconstruction

This irregular three-wave seaway is created by combining a 0.5-inch amplitude wave with a λ/L of 0.7, a 0.25-inch amplitude wave with a λ/L of 1.35, and a variety of 0.5-inch amplitude waves. Specifically, the first 0.5-inch amplitude wave and 0.25-inch amplitude wave are held at constant frequency while the other 0.5-inch wave is varied from a λ/L of 0.5 to two. There are 30 λ/L values tested between 0.5 and two. Each data point is tested twice for a total of 60 runs. The forces and moments as a result of each component wave are then decomposed as described in Section 4.4. The forces and moments as a result of the 0.5-inch wave are then plotted against the single regular wave curve fit and the data is compared. The curve fits and predicted results are also shown for the 0.25-inch amplitude wave which is held constant. The 0.5-inch wave that is held constant is also displayed. The results are shown in Figures 5.15, 5.16, and 5.17. In each graph, red dashed line represents the load versus λ/L curve determined using only 0.5-inch single regular waves and the blue

dashed line represents the 0.25-inch single wave load. The red diamond markers show the contribution of the varied 0.5-inch wave to the forces and moments, and the blue circles represent the contribution of a second 0.25-inch wave to the forces and moments. The black cross-hair style markers represent the forces and moments due to the other 0.5-inch wave which is held at constant frequency.

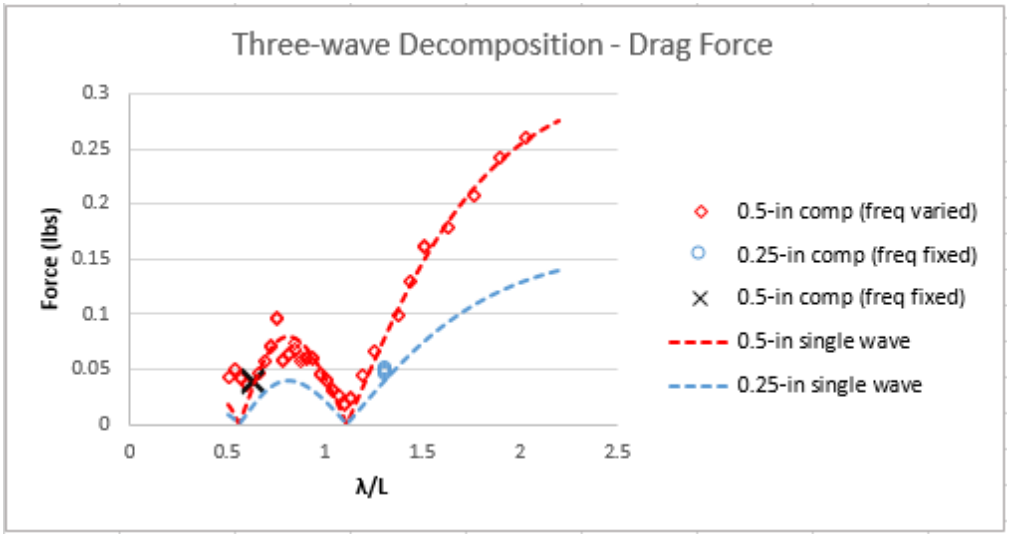

Figure 5.15. Irregular Three-Wave Drag Force

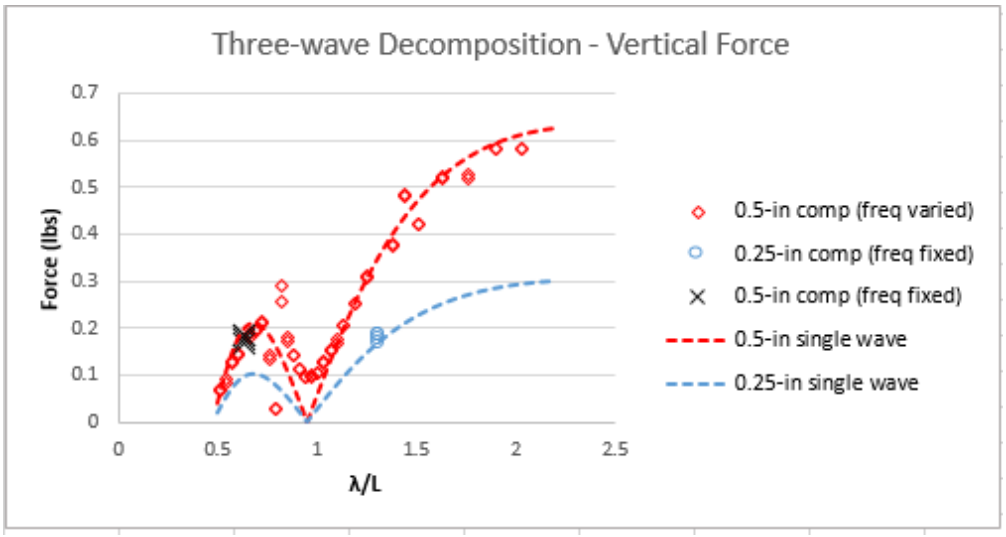

Figure 5.16. Irregular Three-Wave Vertical Force

Again the results appear quite promising, especially when taking into account the uncertainty of the load cell. The load cell has an uncertainty of approximately 0.25 pounds for the

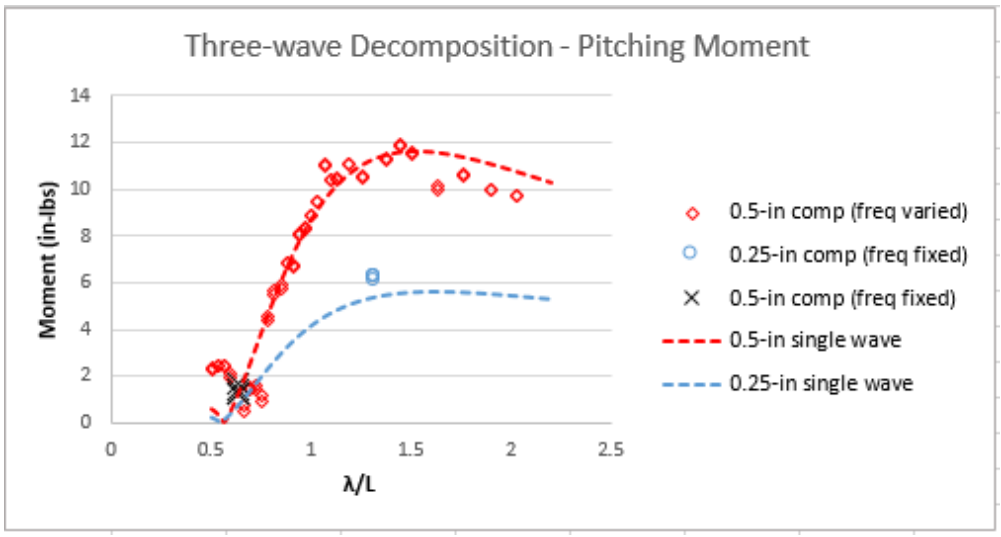

Figure 5.17. Irregular Three-Wave Pitching Moment

vertical force and 2 inch-pounds for the pitching moment. This should be taken into account when analyzing the results. For all three load parameters, the curve fits closely match the experimental data for the 0.25-inch and 0.5-inch waves which were held at a constant λ/L. We see again that for λ/L values greater than one, the single wave curve fits seem to agree with the experimental results. For the drag force, the curve fit under predicts the experimental results for λ/L values near 0.5. At values above this, the data agrees with predictions. For the vertical force, the experimental results agree with the single wave curve fits for λ/L values greater than about 1.05. For λ/L values less than about 1.05 but greater than 0.75, experimental results exceed the predicted values. For λ/L values less than about 0.75, the experimental results agree with the predictions. For the pitching moment, the predictions for data below λ/L values of about 0.75 are close to zero. Thus it is difficult to gain any insight from those values. However, from λ/L values of about 0.75 to 1.5, the experimental results agree with the predictions. For values about 1.5, the curve fits tend to slightly over predict the experimental results.

5.5 Sample Application

A sample application of this data is to predict the force and moment time histories due to complex wave environments. This is done using the RAO transfer function presented in Section 4.8 to single regular wave results and applying linear superposition. The first step

is to calculate the coefficient force value using the non-dimensional curve fit coefficients presented in Figure 5.4 and the λ/L value for the particular single regular wave. For the vertical force this can be done using Equation 2.5. Once the vertical force coefficient value is calculated, the vertical force at any point in time can be calculated using Equation 4.7.

$$F_{z,i} = -C_{fz}\rho g A_o 2w_{a,i}\sin(\omega_i t + \theta_t)$$

Where θ_{tot} is the phase of the incoming wave plus the phase of the force component relative to the incoming wave. Now that the vertical force at any point in time due to a single regular wave is calculated, the process is repeated for the remainder of the wave components utilizing Equation 4.8.

$$F_z(total) = \sum_{i=1}^{n} -C_{fz}\rho g A_o 2w_{a,i}\sin(\omega_i t + \theta_t)$$

A vertical force time history is created in an effort to predict the measured loads in a two-wave component irregular seaway. The first component wave is a 1.0-inch amplitude and 1.52 Hz wave. The second component wave is a 0.5-inch amplitude and 1.349 Hz wave. The predicted time history curves are created over a 10-second interval and then plotted against experimental results. The final plot is shown in Figure 5.18.

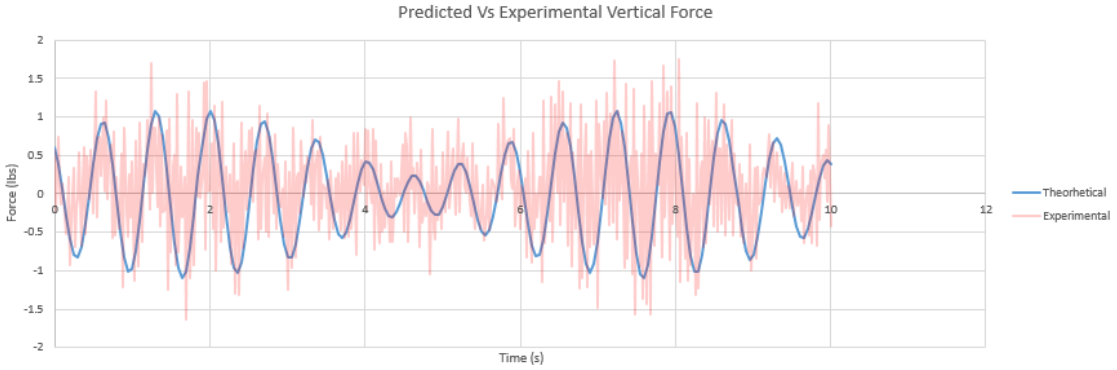

Figure 5.18. Theoretical Versus Experimental Vertical Force Time History

The predicted results do seem to resemble the experimental data. One noticeable difference is the noise in the experimental data. Due to noise, the vertical force signal in the experimental data will always be greater than the predicted results. Regardless, this sample application still appears to be another verification of the use of linear superposition. The RAO process

could be repeated for other parameters such as pitching moment and drag force. The RAO process described here could be very useful in predictive control algorithms by quickly and accurately calculating the short term upcoming force and moment time histories. This could allow control adjustments to be made in anticipation of occurrences of shifting load.

5.6 Potential Limitations

As discussed previously, this experiment was conducted in a laboratory environment under controlled conditions. In the real world, seaways are obviously much more complex than those presented in this study. The first limitation is that the study is only conducted for irregular waves made up of either two to three single regular waves. Ideally, this study would have analyzed five or more single regular waves. The wave making wedge is limited to a travel in either direction of about 3.5 inches and a velocity of no more than 16-inches/second. When combining multiple waveforms with forces and moments large enough to be resolved, these limits can be quite easily exceeded. Thus it was decided to study two and three single wave combinations with large enough amplitudes to be resolved. Regardless, this experiment shows that at least for two and three wave combinations under certain conditions, linear superposition of forces and moments is a valid assumption. Also, this thesis does not consider infinitesimally small waves or breaking waves. All of these could introduce non-linearity into the forces and moments. The experiment was also conducted on a vessel with zero forward speed in head-on seas. More research is required to determine other situations.

The other limitations apply to the scalability of the experiment. This experiment is conducted using a 45-inch long model with a 4.5-inch diameter. Most operational UUVs are larger than this and thus the logical question must be asked of at what size if any the results break down. It appears that these loads are dominated by potential effects and thus it is highly likely that the results will scale up reasonably well. Furthermore, the waves studied range from 0.25- to 1-inch in amplitude. It is unknown up to what amplitude the linear superposition theory is valid.

THIS PAGE INTENTIONALLY LEFT BLANK

CHAPTER 6:
Conclusions and Future Work

6.1 Conclusions

Linear superposition is a valid theory for forces and moments on submerged bodies within the given conditions described in this thesis. The thesis proved this by first analyzing the drag force, vertical force, and pitching moment due to simple regular waves. Each parameter was plotted against the non-dimensional wavelength for various wave amplitudes. A least-squares regression was used to create curve fits in the general form of the Cummins equations [1]. Multiple simple waves were then combined to form complex wave environments and the same force and moment parameters were measured. Once complete, the complex irregular force and moment time history signals were broken down into frequency components that corresponded to the underlying wave components. The resulting data was then compared to the single regular waves forces and moments. It was revealed that the decomposed multiple wave forces and moments closely resembled those for the single regular waves. This shows that linear superposition is a valid theory for the specified example.

In the next phase of the study, the RAO was created, defined, and used to predict force and moment time histories. The connection was made between the RAO transfer function in linear seakeeping theory and non-dimensional force and moment coefficients in this study. Using the RAO transfer function and linear superposition, it was possible to predict the force and moment time histories due to complex waves. Doing so only requires knowledge of the coefficients as well as the amplitudes and frequencies of the component waves. It was also noted that the usefulness of predicting the force and moment time history is likely most beneficial in the design of improved control algorithms as well as testing the validity of linear superposition.

The impact of these results can be realized in a variety of ways. Notably, UUV control systems and control surfaces could be greatly improved for use in near surface operations. It makes predicting the forces and moments due to complex waves much simpler by using information about a bounded set of single regular waves. Because there an infinite number

of possible complex wave environments, this is quite useful.

6.2 Future Work

6.2.1 Speed and Orientation

For the purposes of this experiment, the submerged body had zero forward speed and only experienced head-on seas. The Cummins equations [1] allow for the inclusion of cases other than forward speed and differing wave approach angles with minimal changes to the overall experiment. Further research into the effects of vessel speed and wave approach angle on the superposition of forces and moments is necesary. It is very important to understand such effects before applying the results in this thesis to real world systems.

6.2.2 Number of Simple Waveforms

This experiment has been limited to two and three simple waves to make the complex wave environments. An extensive amount of work remains in the number of regular waves included to build the complex waves. Obviously, more complex waves require more robust wave makers. However, it is possible that a large number of waveforms give rise to non-linearities within the system.

6.2.3 Increased Non-dimensional Wavelength Range

The λ/L of single regular waves in this experiment was limited to a range of approximately 0.5 to 2.0. It is possible to study many λ/L values outside this range in the same manner of this study. A larger λ/L range could be particularly interesting when combining waveforms.

6.2.4 Scalability

Testing the results of this thesis for vessels of varying sizes is another direction one could go. It is unknown if changing the size of the submerged body gives rise to non-linearities in near surface operations. Scalability also applies to the amplitude of the waves in the study. A larger tow tank would likely be required for such a study.

6.2.5 Control System Design

Ultimately, these results could be used as the basis for the design of a UUV control system. In accurately predicting the loads on a shallowly submerged vessel, it is possible to build much better predictive control algorithms. Further research could also lead to a redesign of UUV control surfaces which allow for more efficient near surface operations.

THIS PAGE INTENTIONALLY LEFT BLANK

List of References

[1] W. Cummins, "Hydrodynamic forces and moments acting on a slender body of revolution moving under a regular train of waves," Tech. Rep. 910, 1954.

[2] G. Khalil, "Experimental investigation of wave forces on submerged horizontal cylinders," *Indian Journal of Engineering and Materials Science*, vol. 8, pp. 59–65, Jan 04 2001.

[3] P. Ananthakrishnan and K. Zhang, "AUV motion in a wave field," *OCEANS 1998 Conference Proceedings*, vol. 2, pp. 1059–1063, 1998.

[4] C. Lee and J. Newman, "The vertical mean force and moment of submerged bodies under waves," *Journal of Ship Research*, vol. 15, pp. 231–245, 1971.

[5] J. Pinkster, "Mean and low frequency wave forces on semi-submersibles," *Thirteenth Annual Offshore Technology Conference Proceedings*, pp. 9–14, 1998.

[6] E. Lewis, *Principles of Naval Architecture: Vol. 3: Seakeeping and Controllability*. ociety of Naval Architects and Marine Engineers, 1988.

[7] Short Introduction to Ship Dynamics. Aalto University. [Online]. Available: https://mycourses.aalto.fi/mod/folder/view.php?id=40151. Accessed Apr. 15, 2018.

[8] L. Jones, "Development of a numerical tow tank with wave generation to supplement experimental efforts," M.S. thesis, Naval Postgraduate School, Monterey, CA, 2017.

[9] T. Turner, J. Klamo, and Y. Kwon, "Comparison of wave-induced loads on a near surface slender body from inviscid flow linear solution and an experimental model test," accepted, OMAE 2018 Proceedings.

THIS PAGE INTENTIONALLY LEFT BLANK

Initial Distribution List

1. Defense Technical Information Center
   Ft. Belvoir, Virginia

2. Dudley Knox Library
   Naval Postgraduate School
   Monterey, California